CHALMERS
UNIVERSITY OF TECHNOLOGY

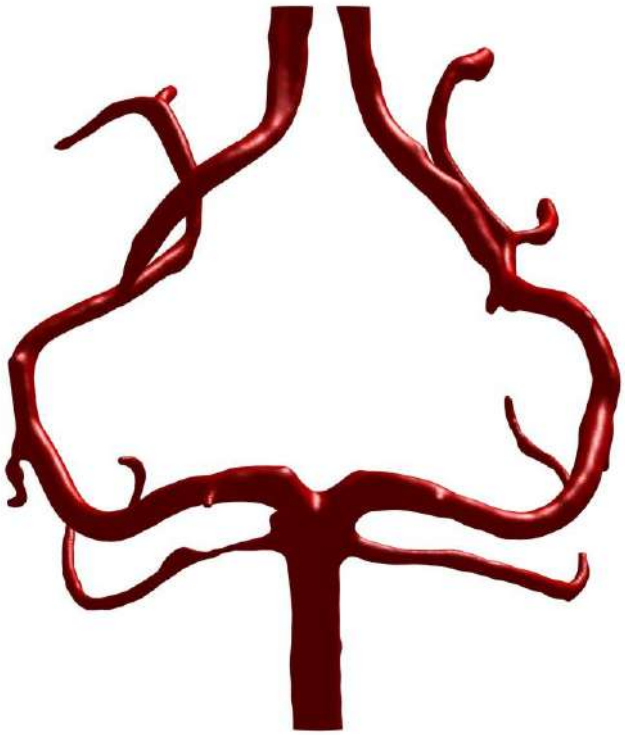

Computational Fluid Dynamics of the Human Cerebral Circulation System

A biological perspective

Bachelor thesis in Mechanical Engineering

Linus Forsman
Ali Mudarres
Isabella Nilsen
Elin Svensson
Samer Talal
Anna von Sydow

DEPARTMENT OF MECHANICS AND MARITIME SCIENCES
DIVISION OF FLUID DYNAMICS

CHALMERS UNIVERSITY OF TECHNOLOGY
Gothenburg, Sweden 2021
www.chalmers.se

BACHELOR THESIS 2021:08
MMSX20-21-14

Computational Fluid Dynamics of the Human Cerebral Circulation System

A biological perspective
Bachelor thesis in Mechanics and Maritime Sciences

LINUS FORSMAN | ALI MUDARESS | ISABELLA NILSEN

ELIN SVENSSON | SAMER TALAL | ANNA VON SYDOW

Department of Mechanics and Maritime Sciences
Division of Fluid Dynamics
CHALMERS UNIVERSITY OF TECHNOLOGY
Gothenburg, Sweden 2021

Computational Fluid Dynamics of the Human Cerebral Circulation System
A biological perspective

LINUS FORSMAN, ALI MUDARRES, ISABELLA NILSEN, ELIN SVENSSON, SAMER TALAL, ANNA VON SYDOW

Bachelor Thesis 2021:08
Department of Mechanics and Maritime Sciences
Chalmers University of Technology
SE-412 96 Gothenburg
Sweden
Telephone: + 46 (0)31-772 1000

Supervisor: Dario Maggiolo, Department of Mechanics and Maritime Sciences
Examiner: Srdjan Sasic, Department of Mechanics and Maritime Sciences

Cover: Reconstructed circle of Willis of patient BH0027

Printing /Department of Mechanics and Maritime Sciences
Gothenburg, Sweden 2021

Abstract

A cerebral aneurysm is a vascular disease causing the structure of arteries to weaken and over time to bulge outward. Rupture of such aneurysms cause intracranial bleeding that can be fatal or significantly impact the patient's life quality. This report investigates the initiation, growth and rupture of cerebral aneurysms. The objective of this thesis is to analyse the biological connection between cerebral aneurysms and the associated blood flow characteristics. By using MRI pictures from a healthy individual's brain, a geometry construction made in MATLAB is used for simulation of the blood flow in arteries using computational fluid dynamics (CFD). The simulations focus on the velocity of the blood flow and the shear stress, and how they vary with different blood models, Newtonian and non-Newtonian, and with and without the presence of an artificial aneurysm.

The results show that areas more prone to develop aneurysms show higher values of shear stress supporting the connection between high wall shear stress and aneurysm initiation. The results also indicate that the presence of an aneurysm affects the fluid dynamics, whose characteristics depend on whether the simulations are based on the Newtonian or non-Newtonian model. In the search of regions at risk for aneurysm initiation, it is suggested that the non-Newtonian model is more preferable in particular due to the ability to include the shear thinning effect.

Sammanfattning

Cerebrala artärbråck (aneurysm) är en kärlsjukdom som försvagar artärens struktur och med tiden gör att den buktar ut. En bristning av ett artärbråck i hjärnan leder till hjärnblödning som kan vara rent dödligt eller resultera i omfattande skador. Den här rapporten undersöker initiering, utväxt och bristning av cerebrala artärbråck. Syftet med uppsatsen är att analysera den biologiska kopplingen mellan cerebrala artärbråck och dess karaktäristiska blodflöden. Genom att använda magnetröntgenbilder från en frisk patients hjärna rekonstrueras en tredimensionell geometri i MATLAB som används för att simulera blodflödet i artärter med hjälp av beräkningsströmningsdynamik (CFD). Simuleringarna fokuserar på flödeshastigheten i artärerna, skjuvspänningen, implementeringen av två olika modeller för blodet, Newtonsk och icke-Newtonsk och med och utan en artificiellt konstruerad aneurysm.

Resultaten visar att områden som är mer sannolika att utveckla aneurysmer har högre skjuvspänning på artärväggen, vilket överrensstämmer med teorin om kopplingen mellan initiering av aneurysm och hög skjuvspänning på artärväggen. Resultaten indikerar också att närvaron av en aneruysm påverkar flödesdynamiken och omfattningen på det beror på om simuleringarna utfördes med Newtonsk eller icke-Newtonsk modell. Vid eftersökning av områden som har högre risk att utveckla aneurysmer föreslås användning av den icke-Newtonska modellen eftersom den tar hänsyn till skjuvförtunningsfenomenet.

Acknowledgement

We would like to begin with thanking our supervisor Dario Maggolio for guiding us throughout this project despite some unexpected changes and group MMSX20-21-81 whom we have collaborated with throughout this project.

Special thanks to all the personnel involved in coordinating this year's baccalaureate despite the many challenges of a pandemic, including the Chalmers Library and Chalmers Writing Center for being incredibly generous with offering their help on the finer details regarding composition of a thesis.

Contents

Nomenclature

Abbreviations

CA	Cerebral aneurysm
CFD	Computational Fluid Dynamics
CoW	Circle of Willis
HB-P	Herschel-Bulkley Papanastasiou
HBM	Herschel-Bulkley model
LBE	Lattice Boltzmann Equation
LBM	Lattice Boltzmann method
NO	Nitric Oxide
NS	Navier Stokes
OSI	Oscillatory Shear Index
PDF	Probability Distribution Function
RBC	Red Blood Cell
SAH	Subarachnoid hemorrhage
WSS	Wall Shear Stress

Fluid Dynamic Units

Bn^*	Bingham number
C^*	Dimensionless consistency $(-)$
k	Flow consistency index (Ns^n/m^2)
l_c	Characterisctic length (m)
M^*	Dimensionless stress growth exponent $(-)$
n	Flow index $(-)$
v_c	Characteristic velocity (m/s)
u	Velocity (m/s)

Greek

$\dot{\gamma}$	Shear rate (s^{-1})
$\dot{\gamma}*$	Dimensionless shear rate $(-)$
η	Apparent viscosity (Ns/m^2)

$\eta*$ Dimensionless apparent viscosity $(-)$

μ Viscosity $(Pa \cdot s)$

μ_c Characteristic viscosity $(Pa \cdot s)$

ρ Density (kg/m^3)

τ Shear stress (Pa)

τ_0 Yield shear stress (Ns^n/m^2)

v_c Characteristic velocity (m/s)

$\tau^*_{mag,av}$ Dimensionless magnitude of shear stress $(-)$

1 Introduction

Stroke is one of the leading causes of death every year, where globally 1 in 4 people over age of 25 have a stroke in their lifetime [1]. In Sweden alone it is the third most common cause of death, costing the country 18 billion SEK each year [2]. The location and severity of the stroke amongst other factors play a big role in how the life quality of the patient is affected. Many may suffer from long term disability and will have to spend the rest of their lives dealing with various cognitive impairments [3] [4].

Stroke is a common term for oxygen deprivation in the brain caused by intracranial vascular diseases, one of which is called Subarachnoid haemorrhage (SAH). In general hemorrhagic strokes are categorized under strokes where a blood vessel ruptures, leaking blood into the space between the skull and the brain, increasing the intracranial pressure [5]. The most common non-traumatic cause of SAH is the rupture of a brain aneurysm, also called a cerebral aneurysm (CA) [6].

This thesis aims to shed light on cerebral aneurysm, its initiation, growth and ultimately rupture. The goal is to provide the reader with a background about the role of blood flow conditions in aneurysm pathogenesis and discuss the underlying mechanical processes. The geometry in focus is the circle of Willis (CoW), which is the main part of the cerebral vascular system that is most susceptible to aneurysm formation [7]. The CoW is a junction of arteries that connects the anterior and posterior blood circulations [8]. Cerebral arteries possess some structural differences as opposed to other types of arteries. Together with many diverging arteries (bifurcations) and structural contortions, they are more vulnerable to local malformation of the blood vessel wall resulting from abnormal blood flow conditions than other blood vessels [7].

1.1 Purpose, scope and objective of study

The field of Computational fluid dynamics (CFD) has since long provided an alternative way of researching cerebral aneurysms. The regulatory effects from mechanical stress on the arterial wall due to blood flow has already been shown in previous studies to be strongly correlated with aneurysm formation, growth and rupture. *In silico* methods such as this provide a less intrusive alternative to not only research, but also evaluate cerebral aneurysms in clinical settings. This thesis could contribute to this field by further consolidating the use of CFD methods, and help towards a more personalised evaluation of patients with such aneurysms. Unlike many other similar studies that include only simplified geometries in their simulations, we have used detailed geometries from MRI.

The theoretical framework is presented by approaching this topic from a biomechanical and fluid dynamics standpoint, and by briefly summarizing the current state of research in this field. Thereafter utilizing this information we conduct a simulation-based study focusing on the shear stress exerted on the arterial wall as a possible discriminator for aneurysm pathology. We show that by reconstructing blood vessels from MRI and by performing numerical simulations via CFD it is possible to realistically describe the complex interaction between the geometrical features of the blood vessels in the CoW. In particular, it is possible to measure the WSS. The implication of two different blood models, Newtonian and non-Newtonian, is also discussed.

The results of the simulations contain data on the average blood flow velocities, and the average magnitude of the shear stress in a single segment of artery from the CoW. In this study the geometries are reconstructed from a healthy patient, using MATLAB to reconstruct the open-source MRI taken from the entire brain. The aneurysm will be added artificially. It is ex-

pected that the flow characteristics will be different in regards to with and without constructed aneurysm. The results will also depend on how the blood itself is modelled, as a Newtonian or non-Newtonian fluid.

The overall objective of this thesis is to analyse the connection between cerebral aneurysms and the associated blood flow characteristics. A simulation-based study is conducted based on the Lattice Boltzmann methodology in collaboration with MMSX20-21-81. They are investigating the hemodynamics of aneurysms in-depth and validate different (CFD) models in order to choose the most suitable one for this project. They provide the simulation results while this thesis focuses on interpreting the data from a biological standpoint, showcasing how the biomechanical responses behind this vascular disease are connected to the dynamic behaviour of blood flow.

2 Properties of Blood

Blood is the fluid in the body that connects every single cell, tissue and organ and is transported through the vascular system. The main components of blood are plasma and cells. The blood volume is 55% plasma which contains 92% water and the rest consists of proteins, ions and small molecules [9]. The cellular elements can be divided into red blood cells (RBCs), white blood cells and platelets. RBCs are the main cellular component of blood and the volume fraction is 45%, they are made of the protein hemoglobin that carries oxygen. White blood cells defend the body against infection and disease. The platelets adhere to the endothelium (the innermost layer of the vessel wall) when injury in the blood vessel wall occurs, and initiate the coagulation process. Other substances transported within the blood are waste products, oxygen, antibodies and chemical messengers such as hormones and proteins. [10]

Blood flow is determined by the pulsating pressure from the heart, the individual flow and mechanical properties of blood and the structure and mechanical properties of blood vessels. Blood flow is pulsatile and can be divided into systolic and diastolic phase. The systolic phase is when the heart pumps out blood and the pressure increases in the outgoing vessels due to contraction of the heart muscle. During the diastolic phase the heart relaxes to refill with blood and the pressure decreases. By measuring the pressure over several complete cycles, the blood pressure can be approximated by a sinusoid. In order to effectively model blood flow, specific assumptions are needed. Although blood is pulsatile, studies have shown that when using population-wide assumptions about the inlet and outlet conditions and material properties, steady flow simulations may substitute pulsatile flow simulations [11]. Under normal circumstances the blood maintains a constant volume, which makes the heart rate proportional to the velocity of blood in the body. When the heart rate increases, so does the velocity, which affects the turbulence and viscosity of the flow. [12]

The viscosity of blood depends on the internal friction between the flow elements and the effects of the suspended particles in the blood. Hematocrit, the volume percentage of RBCs in the blood, also affect the blood viscosity, especially in smaller vessels. Blood viscosity is often approximated 0.035 Pa·s in larger arteries but the viscosity can be higher in vessels with lower shear rates [13]. The value of the viscosity of blood also depends on whether blood is considered a Newtonian or non-Newtonian fluid. When the viscosity increases, more force is required from the heart to maintain the same flow conditions. On the contrary, when the internal friction decreases, the ability of blood to clot will decrease which is a risk when blood vessels are damaged [14].

A Newtonian fluid has a constant viscosity independent of the pressure applied, in contrast to a non-Newtonian fluid that varies. Blood is classified as a non-Newtonian fluid since it varies with the stress. The non-Newtonian characteristics are particularly influential in smaller vessels at low shear stress rates. Another non-Newtonian characteristic in blood is shear-thinning, which implies that the liquids viscosity decreases as stress increases. This is due to RBCs movement in the circulatory system. RBCs have a biconcave shape, similar to a disk, and have high surface area. At lower shear rates RBCs spin around their axis and maintain their original shape, they also have a tendency to aggregate together, often in the form of rouleaux structures [15]. Increasing shear stress leads to more deformation of the RBCs and the rotation around their axis decreases. When the RBCs constitute a smaller volume of the flow, they elongate into ellipsoids and align with the flow, and the viscosity decreases. Figure 1 shows the movement of RBCs in lower shear stress to the left and higher to the right [16]. In case of flow through larger vessels and when the shear rate is above 100 s^{-1}, blood can be approximated as Newtonian [17].

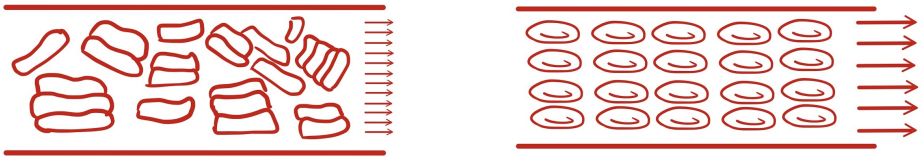

Figure 1: The so called Rouleaux formation, caused by non-Newtonian behaviour of blood (on the left) and the line up during high shear stress (on the right). (Authors' own image)

2.1 Computational Fluid Dynamics of blood

Hemodynamics is the science of blood flow and the mechanics of blood. It clarifies the physical laws that direct the bloodstream within the blood vessels and is therefore a significant element of vascular mechanics and engineering [18]. Blood is a complex fluid, given the growing computational power, the complex fluid dynamics principle describing blood flow and hemodynamics can nowadays be solved at a reasonable time cost, making this research field very appealing. This following section will introduce the concept of fluid dynamics, and how it can be applied in hemodynamics.

Studying the fluid dynamics enables the possibility to determine a fluid's impact on different materials (and vice versa), and the velocity of the fluid flow. Fluid parameters are beneficial to identify in a broad spectrum of industries, including evaluating hemodynamics. Fluid dynamic problems are based on mathematical equations solving the three laws of conservation, conservation of mass, conservation of momentum, and conservation of energy. These mathematical equations cannot always be easily solved analytically in the case of hemodynamics, and therefore a numerical approach must be used. CFD enables solutions to fluid-dynamic problems.

CFD is utilized to solve, analyze and predict fluid flows by using mathematical modeling and numerical methods. There are different possible CFD tools that can be used, the more traditional finite methods and the more recently developed Lattice Boltzmann method (LBM) to name a few. The more traditional methods have been to discretize the Navier–Stokes (NS) equations in a macroscopic continuum. NS equation is a partial differential equation describing the flow of incompressible fluids [19], see equation 1

$$\rho \frac{D\vec{v}}{Dt} = \rho \left(\frac{\partial \vec{v}}{\partial t} + \vec{v} \cdot \nabla \vec{v} \right) = \rho \vec{g} - \nabla P + \mu \nabla^2 \vec{v} \tag{1}$$

were ρ is the density, μ is the viscocity, v is the velocity, g is the gravity constant, t is the time and P is the pressure.

Discretization of the NS equations can be done using different finite methods such as finite difference, finite volume, or finite element methods. The main concept of these methods is to represent the continuous NS equations in a discrete form. Discretization of the NS equations is done by subdividing the domain into cells or elements, expressing the NS equations in discrete form at each point, and solving them using finite methods mentioned above [20]. Using NS equations therefore enables describing the fluid in terms of macroscopic properties, such as velocity and pressure and it allows for modelling of complex geometries.

The LBM is a more recently developed CFD tool. Instead of solving discretised NS equations directly obtaining macroscopic variables. LBM solves discretizations of the Boltzmann equation, so called Lattice Boltzmann's equations (LBE), considering a collection of particles as a unit,

therefore treating the fluid on a mesoscopic scale (in between micro- and macro scale) [21].In order to use the LBM, the discretised LBE is applied along certain vectors (linkages) inside a lattice. These linkages represent the possible paths of a particles collision and movement. Different amounts of linkages and dimensions of lattices can be chosen as the most suitable option for different occasions. The different lattice arrangements are denoted as: DXQY, where X represents the number of dimensions of the lattice, and Y represents the number of linkages (see figure 2).

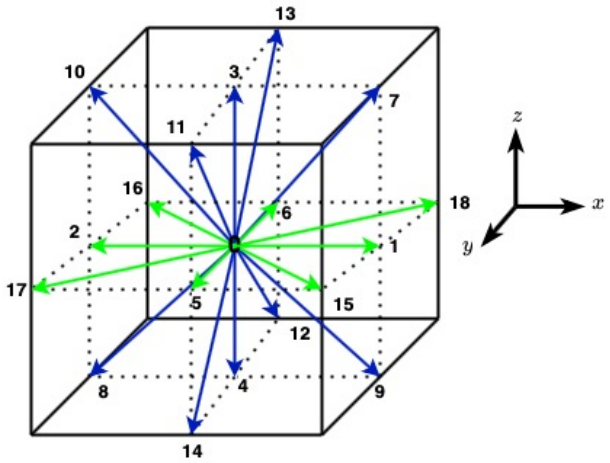

Figure 2: Lattice arrangement with 3 dimensions and 19 linkages (one in the middle included), i.e lattice arrangement D3Q19.

The LBM calculates collision and propagation of the particle's probability distribution function (PDF), solving the Boltzmann equation for particles at each grid point [22]. Macroscopic variables are computed as momentum of the distribution functions, therefore the LBM considers the microscopic dynamics of fluid, while still enabling evaluations of macroscopic fluid dynamics. The LBM approach is a promising solution when dealing with complex flows and geometries because of its inherent computational efficiency [23] [24].

2.2 Hemodynamic discriminators

The following section will define a few hemodynamic discriminators linked to the initiation, growth, and rupture of CA that can be obtained using CFD.

Wall Shear Stress
The Encyclopaedia Britannica defines shear stress as "The force tending to cause deformation of a material by slippage along a plane or planes parallel to the imposed stress", therefore the Wall Shear Stress (WSS) is the force exerted by the fluid on the surface of a wall. In the case of hemodynamics, the imposed stress is caused by the blood flow, and the surface causing the deformation of the fluid is the inside of the blood vessels (endothelium). For Newtonian fluids the shear stress is proportional to the derivative of the velocity according to Newton's law of viscosity:

$$\tau = \mu \frac{dv}{dy} \tag{2}$$

where τ represents the shear stress, and μ the viscosity of the fluid. Non-Newtonian fluids on the other hand, behave differently [25]. The shear stress for a non-Newtonian fluid can be expressed by different models, such as the Herschel-Bulkley model (HBM), that combines the shear thinning effect, and thickening properties. This enables the modelling of yield stress with viscosity depending on shear rate, see equation 3

$$\tau = k\dot{\gamma}^n + \tau_0 \tag{3}$$

where n is the flow index, k is the consistency index, $\dot{\gamma}$ is the shear rate, $\dot{\gamma}$ and τ_0 is the yield shear stress. Another model that can be used is an extended version of HBM, the Herschel-Bulkley Papanastasiou (HB-P) equation

$$\tau = k\dot{\gamma}^n + \tau_0 \left(1 - e^{-m|\dot{\gamma}|}\right) \tag{4}$$

where m is the stress growth exponent. This equation is very suitable for simulation of blood since it not only combines shear thinning and thickening properties like the HBM, it also applies in both the unyielded and yielded regions of the blood, and according to our cooperating group, MMSX20-21-81, the HB-P is sufficient enough to use in the simulations [26].

Oscillatory Shear Index
OSI is a dimensionless measure of changes in direction of shear forces on the vessel wall during the cardiac cycle [27], it provides information on whether or not the WSS vector is aligned with the time averaged WSS vector throughout the cardiac cycle . The OSI can be calculated using the following equation

$$\mathbf{OSI} = \frac{1}{2} \cdot \left(1 - \frac{\left| \int_0^T \vec{\tau} dt \right|}{\int_0^T |\vec{\tau}| \, dt} \right) \tag{5}$$

where $\vec{\tau}$ represents the WSS vector and T represents the time period of the cardiac cycle.

In the present thesis we do not measure the OSI, but we recognise that it may play an important role in the growth and rupture of aneurysms.

2.3 CFD and hemodynamics

Investigating the risk of rupture of an aneurysm is important since treatments used today, such as surgical clipping and implementation can increase the risks of bleeding, stroke, and vessel spasm and therefore want to be avoided [28] [29]. CFD technology provides measurements of various hemodynamic parameters, once certain correlations between the hemodynamic parameters and aneurysm rupture have been identified, minimally invasive risk assessments of aneurysms can be made. CFD is based on calculations, meaning it is also possible to predict flow for certain geometries that not yet exist. Surgical treatment results in a change of geometry, therefore CFD provides the ability of studying the risks of certain surgeries before they have been done [30].

3 Theory of Cerebral Aneurysms

A cerebral aneurysm (CA) or simply brain aneurysm, is a vascular disease causing the structure of mainly arteries to weaken and over time to bulge outward. There are two distinct shapes of CA, fusiform and saccular (see figure 3). In the CoW, the saccular shape is the most common type of aneurysm. The two shapes have different pathological processes and are medically treated differently [31]. For the remainder of this section and upcoming sections, the focus will only be on saccular aneurysms.

Although life threatening when ruptured, the majority of brain aneurysms remain dormant. About 2 % of the general population carry some form of unruptured brain aneurysms that have low risks of bursting. However, the SAH stands for more than 5 % of all stroke cases, with a mortality rate of somewhere between 30-40 %. Up to 70 % of those who survive will suffer from serious short-term cognitive impairments while 59 % of those never fully recover. It is clear that once a brain aneurysm ruptures, devastating consequences will follow that significantly impacts the patient's life quality [32] [33].

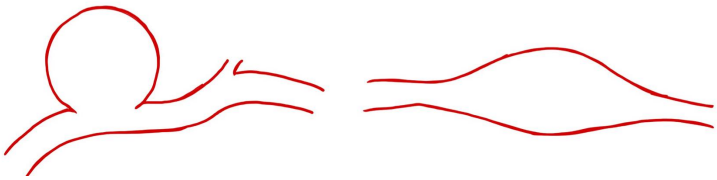

Figure 3: Two types of aneurysms. One sticking out from one side of the artery with a neck and dome called saccular (left) and one uniformly bulged on all sides called fusiform (right). (Authors' own image)

There has been attempts at forming generalized rupture risk assessment protocols [34], [35], [27], [36], [37], [38]. Rupture risk can depend on many factors, everything from hemodynamics of the aneurysm, its size and location, genetic and environmental factors, irregularities of the aneurysmal vessel and so on [31]. From a pure size perspective, saccular aneurysms with diameters less than 3 mm have a low risk of rupturing, while the risk increases more significantly for diameters bigger than 7 mm. For diameters between 3-7 mm the risk assessment becomes less precise, requiring more parameters to be factored in and the evaluation needs to become more personalised [33] [31]. Mechanism of aneurysm initiation, growth and rupture are still not completely understood to this date [39] [40]. There are numerous studies with different approaches, mainly *in silico* and *in vivo* using a variety of models and measuring methods that consequently has led to contradictory results on how the flow environment triggers the CA pathogenesis [36]. In the upcoming sections, we will present the most well-known theories linked to different stages of CA pathophysiology [32] [33].

3.1 Structure of Cerebral arteries

The artery wall consists of three main layers, see figure 4. The outermost layer is called the tunica externa and consist of connective tissue which helps the artery to attach to surrounding tissue in the body. The middle layer is called the tunica media and mainly consist of smooth muscle cells. Smooth muscle cells are used by the nervous system to control functions such as food digestion in the stomach or in this case, blood pressure in the arteries. Lastly, the inner-

most layer which is called the tunica intima. It consists of endothelial cells and the internal elastic lamina.

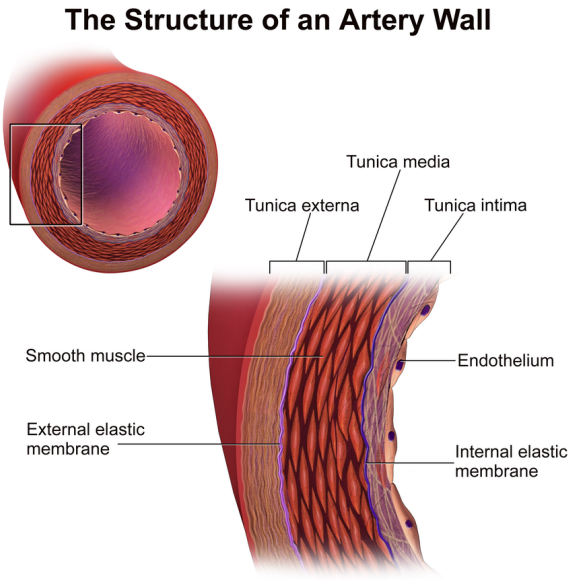

Figure 4: The anatomy of the arterial wall [41]. CC-BY.

Endothelial cells are a cell type that covers all kinds of organs and structures within the body [42]. The internal elastic lamina is a boundary sheet that separates tunica intima from tunica media. It is more developed in cerebral arteries which instead lack the external elastic lamina that is a part of the outermost layer in other systemic arteries [43]. These features place the cerebral arteries at a higher risk of developing aneurysms [44]. This innermost layer of the artery wall has shown to play an important role in the development of aneurysms. Damage or injury to the innermost layers is the first step in the formation of aneurysms [45]. In the next section, we are going to explain the mechanisms behind the dysfunction of endothelial cells and the initiation of aneurysms.

3.2 Aneurysm initiation

Examples of risk factors for developing aneurysms include alcohol consumption, hypertension and smoking. These factors contribute to the generation of reactive oxygen species, causing oxidative stress. This damages the endothelial layer by making it more permeable, i.e easier for molecules in the vessel to pass through the wall. Toxic chemical reactions in combination with hemodynamic forces can lead to the development of aneurysms.

Since there is a constant pulsating blood flow in the vascular system there has to be a balance between the hemodynamic force and the vessel wall to not cause any dysfunctions. When artery walls are exposed to abnormal hemodynamic stress, several studies show that it can in some cases cause dysfunctions of the endothelial cells [45] [46]. The force of WSS acting on a healthy aorta can range between 1 and 2 Pa. In smaller arteries like in cerebral arteries the value increases marginally, an effect of smaller diameters [45] [47].

The WSS has also shown to increase around artery bifurcations and vessel bends due to the development of increased flow velocity in these locations. These areas are thereby more vulner-

able to endothelial dysfunction [48]. Further, studies have found that these artery wall areas are uneven in structure, and thereby more prone to endothelial dysfunction which further could explain why the initiation of CA mainly occurs in artery bifurcations and bends [49].

When cells are exposed to hemodynamic stress they try to balance this with several linked reactions. For instance, a hazardous nitric oxide (NO) synthase activity occurs. High shear stress leads to an increase of synthesized NO. Among several things NO prevents smooth muscles from tightening and mediators, that cause inflammation. With the help of NO, the smooth muscles inside the artery relax and the vessel expands. This process lowers the WSS and prevents injuries to the vessel wall. Although in abnormal conditions when the artery already has suffered from some sort of disruption a dramatically increase of NO take place which is toxic to the cell wall [45]. These disruptions could be as earlier mentioned in the section, caused by smoking or hypertension. Estrogen is a hormone that also helps to upregulate the synthesis of NO to protect the vessel wall. In the case of estrogen imbalance, the same process as described above could occur.

The endothelial cells are bound together by junctions. Previous studies have shown that in the early stages of aneurysm initiation morphological changes of these junctions occur in arterial bifurcations. This leads to a gap formation in between the cells that allows leukocytes (white blood cells) to migrate in between the gaps. The result of this process in the long run is an outward bulging of the arterial wall, i.e an aneurysm is formed [45].

Another theory for the initiation of aneurysms is energy loss. Energy loss as a biomechanical parameter describes how much energy is absorbed by the artery during the cardiac cycle. During systole the artery expands, storing energy and shrink backs to normal size during diastole returning this energy to the blood. There is a link between this parameter and the imbalances in elastin and collagen composition on the artery. Once the energy dissipation becomes greater than normal, the blood vessel could undergo wall remodelling which initiates aneurysms [50].

3.3 Aneurysm growth & rupture

Data regarding aneurysm growth and rupture has a high degree of variation and suffers from small studies with different modalities [30], [31], [39], [51], [52]. The lack of consensus originates from a lack of standardization of procedures, e.g. the method of processing the input values and simulations varies highly between research centres. Incorrect annotations for different hemodynamical parameters, lack of discrete definitions and the choice of different models all complicate statistical analysis and interconnection between various studies in the field. Here we present a brief overview of biological and hemodynamic factors that may be used to assess aneurysm growth and rupture risk.

So far the association between hemodynamic factors and the biological response is limited to *in vivo* and *in vitro* studies which limit the clinical application on humans but offer useful insight on how the physiological responses work and how it reacts to medication [51]. Rupture discriminators can be divided into two groups, geometry and flow dynamics. The discriminators and risk factors, which are similar between the growth phase and rupture of aneurysms, are here presented and discussed.

3.3.1 Aneurysm growth

To begin with aneurysm growth, studies have found that complex intrasaccular flow patterns sustained an environment important for aneurysm growth [53]. The following discriminators were found to be statistically significant

- Shear rate ratio (average aneurysm shear rate, a measure of the deformation of the fluid elements, divided by the average shear rate of the parent artery).
- Vorticity ratio (ratio of the average aneurysm vorticity, a measure of the rotational velocity of fluid elements, over the average artery vorticity).
- Viscous dissipation ratio (amount of viscous energy dissipation in the aneurysm with respect to that in the parent artery).
- Shear concentration index (degree of concentration of the WSS distribution).

The environment predisposing aneurysm growth could be explained by the complex intrasaccular flow patterns resulting from concentrated inflow streams. This complex pattern induces nonuniform WSS distributions with areas of concentrated high WSS and large areas of low WSS. Other studies suggest categorizing aneurysm growth into focal and global types and then measure the discriminators such as WSS [52]. For focal types (formation of blister or daughter aneurysm on the original aneurysm) high local OSI and low WSS was observed while high WSS and larger WSS gradient affected global aneurysm growth [54] [55].

3.3.2 Aneurysm rupture

In general factors such as aneurysm diameter, location, surface area, shape irregularity and aspect ratio (the quotient between perpendicular aneurysm height and neck diameter) are among the geometric factors that played a significant role in study of ruptured aneurysms [56]. On the other hand, there is WSS, OSI, low shear area, relative residence time (how long the blood remains near vessel wall, calculated from WSS and OSI) etc as flow dynamic factors. Several studies have suggested low WSS to be a contributing factor to aneurysm rupture [51], [57], [58], [59]. By simulating multiple aneurysms in the anterior and posterior part of CoW, Berg and Beuing found that low WSS, high oscillatory stress and unstable flow were present in ruptured aneurysms.

Inflammation plays an important role in aneurysm growth and rupture, supported by observation of the positive effects of taking the anti-inflammatory medicine aspirin [60]. The low WSS values have been shown to trigger a process called leukocyte extravasation, which is the recruitment of white blood cells from the blood stream into the endothelium of vessels triggering inflammation. Overall the integrity of blood vessel structure in presence of an aneurysm seems to be greatly impaired by chronically low WSS [59].

Small thin-walled aneurysms have different discriminators than large and atherosclerotic aneurysms [39]. The former associated with high WSS where mural cells (important for vascular development and stability) activate proteases causing significant damage to the internal elastic lamina. This ultimately leads to bulging of the vessel that ruptures due to high WSS and inflow velocities. Low WSS on the other hand as explained earlier activates cell-mediated inflammation affecting larger aneurysms where the blood normally has a high relative residence time.

3.4 Circle of Willis

The majority of CA are found in the circle of Willis, named after the physician Thomas Willis due to his many contributions to neuroanatomy [61]. Through CoW the anterior and posterior blood circulation is connected in such a way that in cases of vascular malfunctions other arteries in the area can take over and compensate for the compromised flow [62]. See figure 5 for a general illustration of the vascular anatomy of the brain. In should be noted the human population exhibit a variety of anatomical differences of CoW, thus this anatomical model is a generalisation of this vascular system. The following sections will provide the framework regarding the selection of geometries used in blood flow simulations.

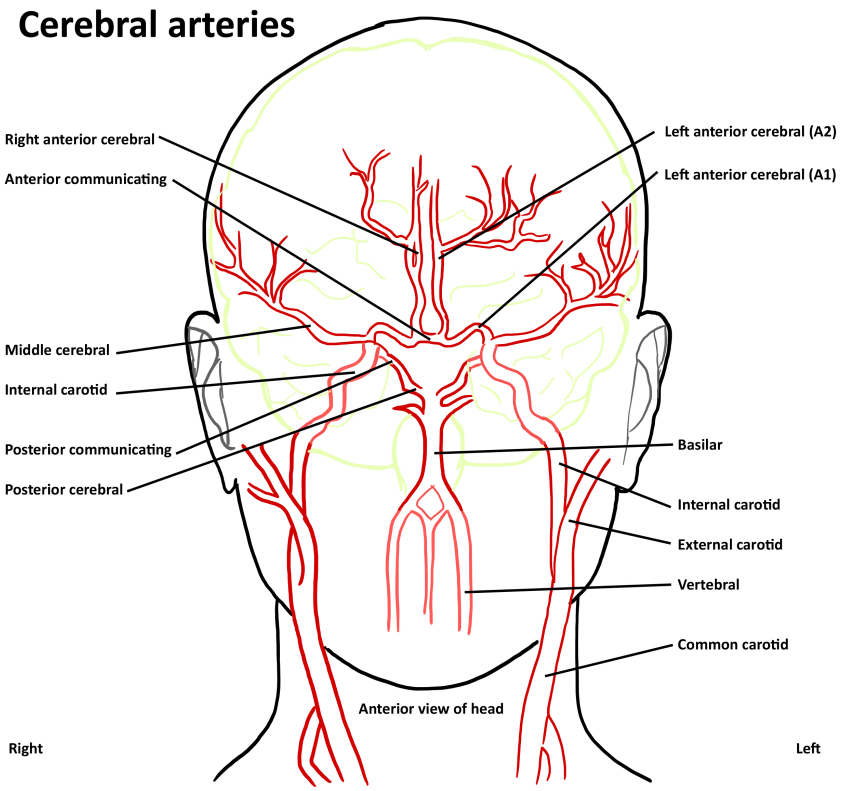

Figure 5: Anatomy of the human cerebral vascular system. At the base of the brain sits the area called circle of Willis, viewed from the front (anterior) of the head. (Authors' own image)

3.4.1 Anatomy and variations

Situated at the base of the brain, CoW is a circular bridge composed of various arteries. Divided into two main parts, the top part includes the interior blood circulation while the lower half makes up the posterior part of the circulation situated near the stem of the brain, see figure 6. The internal carotid arteries are responsible for blood supply to the frontal lobes, parietal lobes and lateral temporal lobes. Meanwhile, the vertebral arteries supply the brainstem, cerebellum, occipital lobes and medial temporal lobes. The posterior communicating artery connects the middle cerebral artery with the posterior cerebral artery [63]. It is in this artery that 15-25 % of all brain aneurysms have been found, all of which are more prone to rupture compared to other locations [64]. The ability of CoW to reroute the blood flow in case of damaged arteries varies from person to person due to anatomical variations. It may also play an important role

in rupture of aneurysms [65] [66]. The two most vital arteries in this rerouting mechanism are the anterior communicating artery and posterior communicating artery although secondary pathways exist if these arteries are compromised [64]. Studies ranging between 500+ and 50+ number of patients have been conducted that support the vast anatomical differences and their connection to cerebrovascular diseases [67], [68], [69]. For the sake of simplicity, only one such work has been included here that presents a comprehensive overview. It is backed by both literature research and examination of computed tomography angiography (CT angiography) pictures done by Bruno Coulier. See figure 7 for common segments that are missing or are malformed in the general population. Coulier observed a general trend of a lower percentage of complete CoW structure in patients suffering from cerebrovascular diseases [67]. The following section will address the correlation between anatomical differences of CoW and CA rupture.

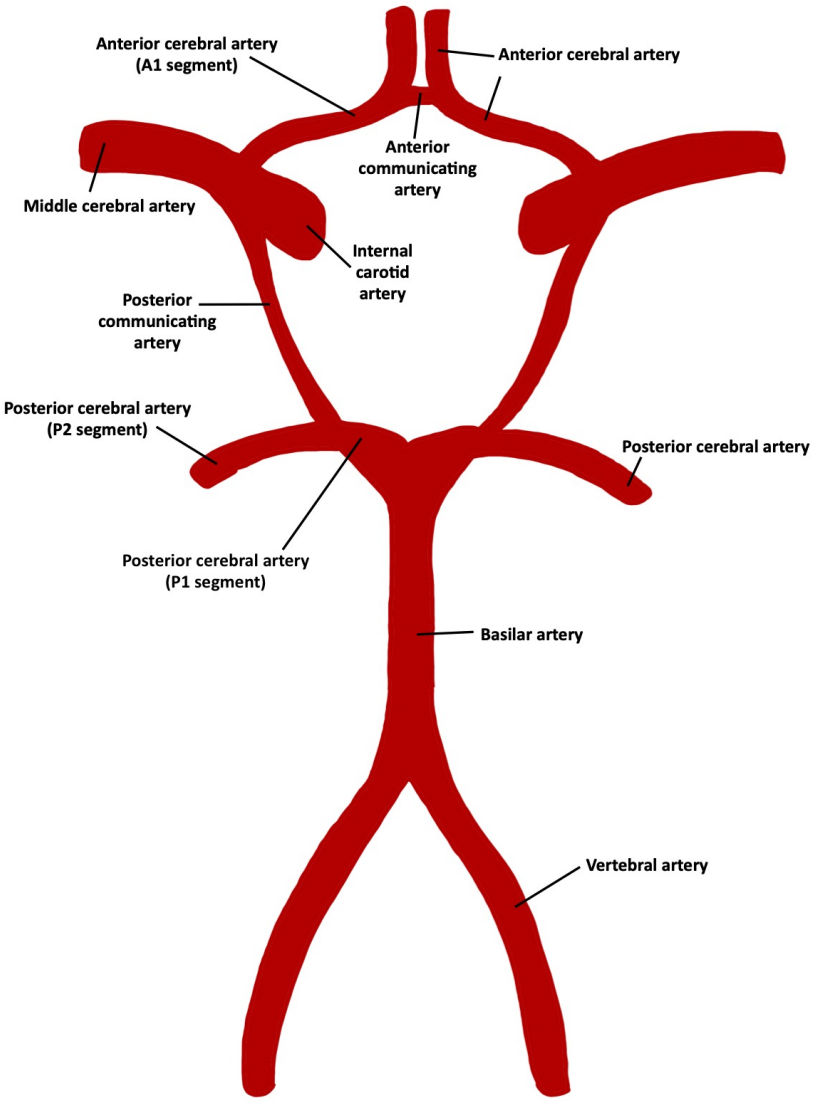

Figure 6: A detailed anatomy of the CoW together with names of different segments. Source: Authors' own image

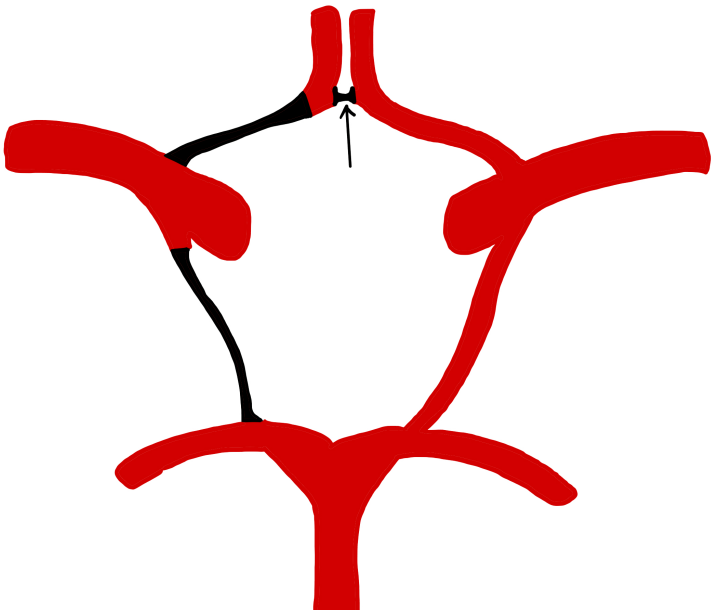

Figure 7: Only 6 % had robust CoW configuration according to the study by Bruno Coulier. The illustrated segments above are the common places which malformations can occur. Source: Authors' own image

3.4.2 Connection with Aneurysm rupture

As discussed in previous sections, elevated or very low WSS are the two main hemodynamic factors that contribute to aneurysm formation, growth and rupture. These are the forces behind vessel wall dysfunction giving rise to cascades of biomechanical responses, chemical reactions and ultimately remodelling of the arterial wall structures. One way abnormal pressure distribution can come to exist is the asymmetry in CoW, causing asymmetric flow distribution. Thus, paths of higher blood pressure in certain arteries can occur more than others [70] [65]. A study done by Xu et al. demonstrated that one cause of elevated levels of WSS was connected to an anatomical variation of CoW, namely the fetal-type posterior cerebral artery [64]. Normally blood flows into the posterior communicating artery from the posterior cerebral artery. The inchoate section of the posterior cerebral artery (the P1 section in figure 6) caused the blood flow to be redirected and supplied from the internal carotid artery instead, resulting in increased blood pressure at the bifurcation [71]. Upon the formation of an aneurysm the nerves responsible for the movements of the eyes could be pressed or crippled entirely resulting in vision problems during the growth and rupture phase. This can even serve as a warning sign prior to aneurysm rupture [72].

Another study with approximately half the amount of subjects investigated the general connection between CoW structures and aneurysm rupture [65]. They found that an underdeveloped or overdeveloped A1 segment of the anterior cerebral artery (see figure 6) was directly connected to the rupture of CA. Since blood flow is impaired in the A1 segment, it would increase through the anterior communicating artery to compensate which would increase pressure and shear stress at the junctions, triggering different aneurysm formation, see figure 8.

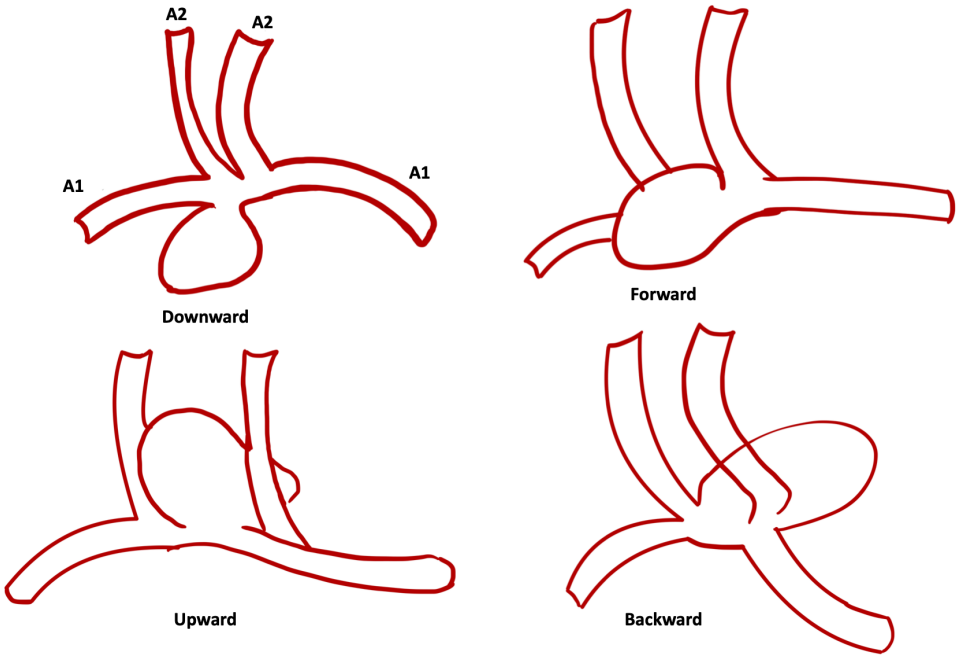

Figure 8: Common ways aneurysms can form at the anterior communicating artery. (Authors' own image)

4 Method

This section describes the method used to reconstruct the geometry and the CFD calculations and simulations. The reconstructions and simulations were done cooperatively with MMSX20-21-81. Since this thesis focuses on biomechanics rather than fluid-mechanics, we will use the conclusions regarding the appropriate mechanical basis of the blood flow, appropriate lattice, CFD method, and validation of said method obtained by group MMSX20-21-81 [26]. As discussed in the previous chapter, the exact geometrical configuration of the blood vessels can play an important role in determining aneurysm growth and rupture. In the present work, we thus reconstruct blood vessel geometries from MRI to fully reconstruct three-dimensional vessel morphologies in the CoW.

4.1 Method for geometry reconstruction and selection

To reconstruct a 3D geometry of the human cerebral circulation system, MRI scans from two human brains, called BG0001 and BH0027, were processed in MATLAB. With the help of Image Processing Toolbox in MATLAB, data from the dicom files of the 2D MRI scans were read and stacked on top of each other creating a 3D matrix. The data contained in this matrix includes data of the whole brain thus requiring a method for the extraction of the cerebral circulation system. The method chosen was thresholding. The principal of thresholding is that different tissues in the brain gives different intervals of pixel intensities. Therefore by setting all pixel intensities lower than a manually chosen threshold value to zero, the cerebral circulation system could be extracted. The advantage of thresholding is its easy implementation, the disadvantage is that some tissues share parts of the same pixel intensity intervals, creating an overlap of different tissues in the extraction. In our case, bone and blood vessels partly shared the same pixel intensity values [73].

The next step was filtering out small volumes and plotting the filtered image. This created a clear 3D geometry from which the CoW and other interesting parts could be identified. The disadvantage of thresholdning, showing parts of the skull in our case, did not affect the whole 3D geometry. The interesting parts did not contain any bone fragments thereby clear images could be extracted, see figure 9.

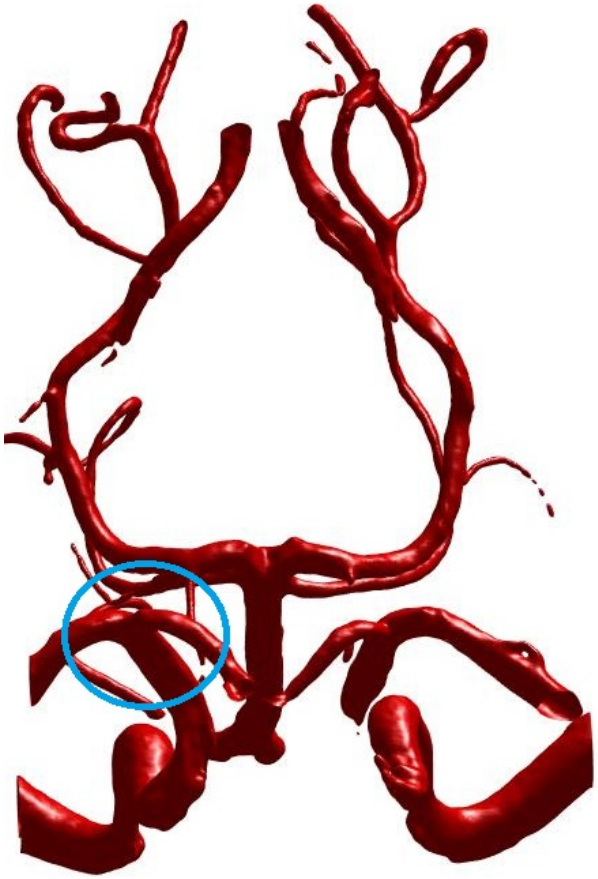

Figure 9: CoW of BG0001. The blood vessel marked with a blue circle is the Internal carotid artery used in the simulations.

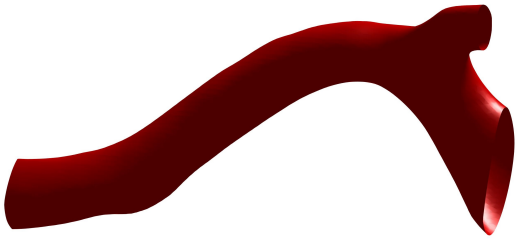

Figure 10: Internal carotid artery of BG0001 used in the simulations.

For the simulation the internal carotid artery was extracted from BG0001. The reason being that it has a bifurcation with a large parent vessel and two large daughter vessels, making it an interesting geometry to simulate, see figure 10.

When taking out the different geometries that were of interest, the selection was limited by a number of causes. In order to simplify the setup for the simulation, which will be discussed in later sections, the arteries that were taken out from the plot of the CoW had to begin and end in the same plane in the 3D plot. For instance if a geometry was taken out such that the artery was cut in the XY-plane the end had to be cut in the XY-plane too. The artery was also limited to be preferentially aligned along one specific direction. These limitations led to a number of arteries not being able to be constructed for the simulations. The selected arteries are therefore

the ones that meet the criteria for the simulations and matches the description of being at risk for aneurysm as mentioned in section 3.

The simulation requires a steady state of the flow for the result to be closer to what it would have been in reality. This means that the simulation must be long enough to allow steady state to development. This was done by creating an artificial vein in MATLAB using the formula for a circle to create segments of circles on top of each other with increasing or decreasing radius. This allows the outlet of the artificial vein to match with the inlet.

The two patients BG0001 and BH0027 are healthy patients in the manner that no evolved aneurysm has been detected on them. For the purpose of this thesis the simulation should include geometries with arteries that has an aneurysm. This lead to creating fake growth of aneurysm in MATLAB in the same way that the artificial veins were created, see figure 11. The result of an artery with both the artificial vein and a created aneurysm growth are shown in figure 12. This was done so the result could be compared with the results from a geometry without the added aneurysm.

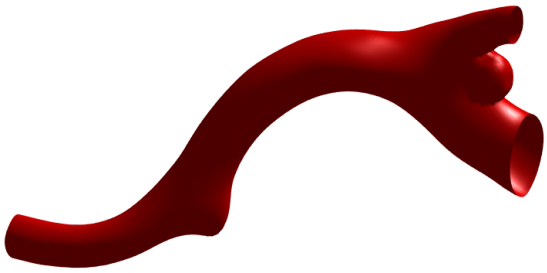

Figure 11: Internal carotid artery of BG0001 with a constructed aneurysm used in the simulations.

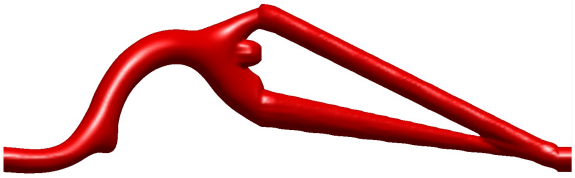

Figure 12: Internal carotid artery used for simulation from BG0001

4.2 Assumptions and flow conditions

A large part of the fluid-mechanics studies regarding hemodynamics assume the blood flow to be Newtonian. However, blood as well as many other fluids encountered in real scenarios, or industry do not express the linear relationship between shear stress and viscosity. In the case of a shear thinning fluid, such as blood, it is necessary to model accurate shear-dependent variations in viscosity. This was done by making new models with non-Newtonian fluids. To choose the most accurate model is very important when it comes to risk assessments, since over- and underestimations of WSS can have a significant effect on the patients medical profile. The two different models, Newtonian- and non-Newtonian are compared and reflected on in the result section.

Generally the blood flow in arteries is laminar. However, under certain conditions such as the branch point at big arteries, the flow becomes more chaotic resulting in a high loss of energy via turbulent mechanisms. Since the cerebral arteries are small, the model is made to meet the laminar criteria. During this project some assumptions had to be made in order to proceed with the simulations. The flow would be considered laminar throughout the simulation and the vessel-walls were assumed to be rigid walls.

4.3 Simulation of LBM

The Lattice Boltzmann simulations are performed for a Newtonian and non-Newtonian fluid described by the Herschel-Bulkey model, see equation 4. The HB-P model was chosen since it is important to include the change of yield stress of a fluid due to the risk of receiving shear stress values that differ from the actual value. This leads to faulty assumptions of the blood flows discriminating values. Due to the risks of surgical treatment of aneurysms, and the risks of rupture if critical aneurysms are left untreated, it is crucial to acquire accurate results. Any over- or underestimations of the discriminator values should be eliminated. Table 1 presents the most suitable characteristic parameters for the CoW. These have been verified by our cooperating group, MMSX20-21-81 [26], and are therefore used in the simulations. In dimensionless form, the HB-P model is described by the parameters reported in table 2. With such parameters, we confidently mimick a realistic blood flow condition, with shear thinning and yield stress taken into account.

Table 1: Characteristic parameters.

Parameter	**Label**	**Value**
Density	ρ	1000 kg/m^3
Viscosity	μ_c	0.004 Ns/m^2
Length/mean diameter	l_c	3.08 mm
Reynolds number	Re_c	40
Yield stress	τ_0	0.04 N/m^2
Flow index	n	0.95
Consistency index	k	$1.712 \cdot 10^{-2}$ Ns^n/m^2

Table 2: Defined dimensionless parameters.

Dimensionless parameter	**Description**
$C = \frac{k}{\mu_c}\left(\frac{v_c}{l_c}\right)^{n-1}$	Dimensionless consistency
$Bn = \frac{\tau_0}{\mu_c}\frac{l_c}{v_c}$	Bingham number $= \frac{\text{yield stress}}{\text{viscous stress}}$
$M^* = \frac{Mv_c}{l_c}$	Dimensionless stress growth exponent [74]
$\dot{\gamma}^* = \frac{l_c\dot{\gamma}}{v_c}$	Dimensionless shear rate
$\eta^* = \frac{\eta}{\mu_c}$	Dimensionless apparent viscosity

The HB-P model (equation 4) can be written as

$$\eta(\dot{\gamma}) = \frac{\tau}{\dot{\gamma}} = k\dot{\gamma}^{n-1} + \frac{\tau_0}{\dot{\gamma}}\left(1 - e^{-m|\dot{\gamma}|}\right) \tag{6}$$

when inserting the dimensionless parameters listed in table 2, the HB-P can once again be rewritten as

$$\eta^*(\dot{\gamma}^*) = C|\dot{\gamma}^*|^{n-1} + \frac{Bn}{|\dot{\gamma}^*|}\left(1 - e^{-M^*|\dot{\gamma}^*|}\right) \tag{7}$$

using these dimensionless parameters enables a simpler form of the equations. A reduction of number of variables can be obtained when dimensions cancel each other out. It also makes it possible to conduct a simpler comparison between experiments with different variables, giving scaling laws that easily can be examined. The dimensionless values are computed using some

characteristic physical parameters typical for blood flow description, such as vessel diameter and blood viscosity. Therefore, the dimensionless values allows a direct comparison between the simulated data and such more simplistic values.

The lattice arrangement used in the simulations is D3Q19 (see figure 2), meaning a cube with 19 linkages was chosen as the most optimal arrangement for simulating blood flow [24]. The simulation of blood flow was done in the chosen geometries extracted from the MRI explained in section 4.1.

5 Results

The following result was obtained from the chosen and reconstructed geometries with the use of numerical methodology explained in section 4.3. It presents how the dimensionless shear stress, dimensionless average shear stress, and the average velocity varies for the different models. The results are displayed in two different types of figures where one shows the geometry in 3D, and the other is a graph showing how the average shear stress or the average velocity varies in a specific cross-section of the artery. It should be noted that due to the use of dimensionless parameters, the values obtained in the graphs are only representative when conducting comparative studies between the different simulation-alternatives.

5.1 Comparison of shear stress in geometries with and without constructed aneurysm

Fake aneurysms were created to evaluate its effect on the blood flow. The aneurysms were placed in the bifurcations since it is the most common spot for aneurysm initiation, as stated in section 3.2. Figure 13 and 14 illustrate the distribution of shear stress in the artery wall from patient BG0001 when simulating blood as a Newtonian fluid with and without the aneurysm, whereas figure 15 and figure 16 show the simulations of blood as a non-Newtonian fluid with and without the aneurysm.

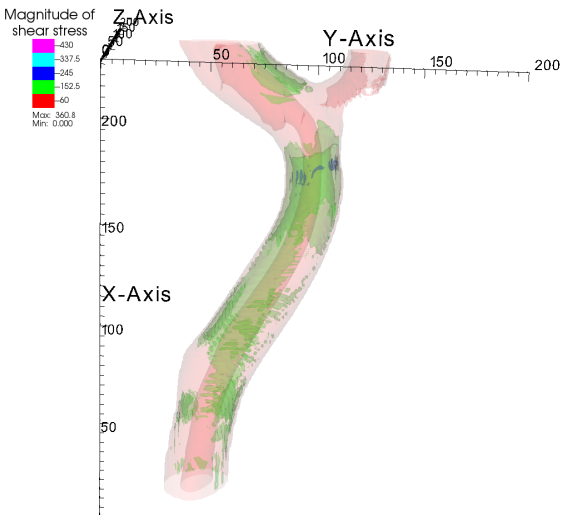

Figure 13: Newtonian without aneurysm

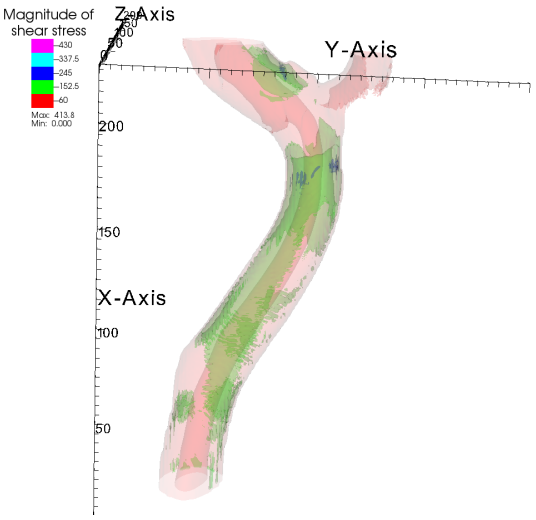

Figure 14: Newtonian with aneurysm

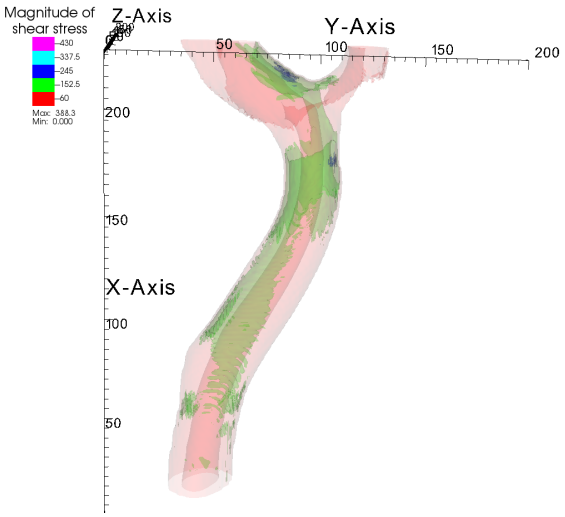

Figure 15: non-Newtonian without aneurysm

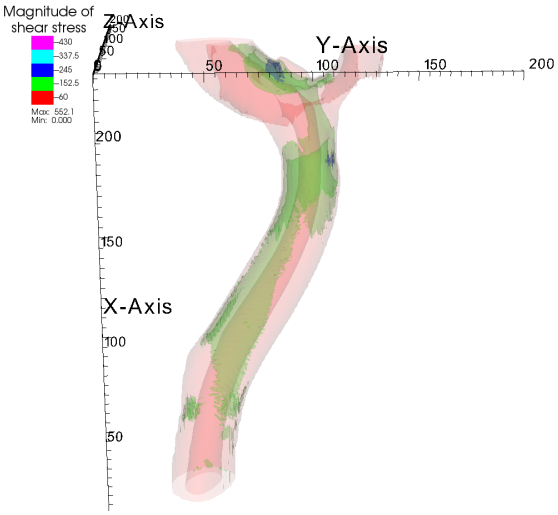

Figure 16:
non-Newtonian with aneurysm

It should be noted that the entire aneurysm is not visible in figure 14 and 16 because the shear stress is too low at the top of the aneurysm and is colored as white. For reference see Figure 17 which shows the full size of the aneurysm to the left, and the full size of the artery without the aneurysm to the right.

Figure 17: Artery from patient BG0001 with and without aneurysm.

From the four 3D-plots of the artery it is possible to see an increase in shear stress on the left side of the bifurcation when adding the aneurysm. The maximum value of shear stress in both blood models increases when the aneurysm is added. Although it is not entirely easy to capture these variations in the 3D plots due to the small area they act on. For this reason some cross-sections near and including the aneurysm will be presented separately in the following results.

5.1.1 Comparison of shear stress in cross-sections with and without constructed aneurysm

The following graphs representing obtained values from cross-section analysis are computed along the z-axis. Since it can be difficult to grasp the direction of the z-axis and the location of the cross-sections figure 18 and 19 are provided to aid the visualisation. When reading the following graphs from left to right, one reads the values from the vessel from left to right in figure 18 at the specified cross-section, represented by the black lines in figure 19, where the bottom cross section in the figure is at x=160, middle one at x=205 and the top cross section is at x=217.

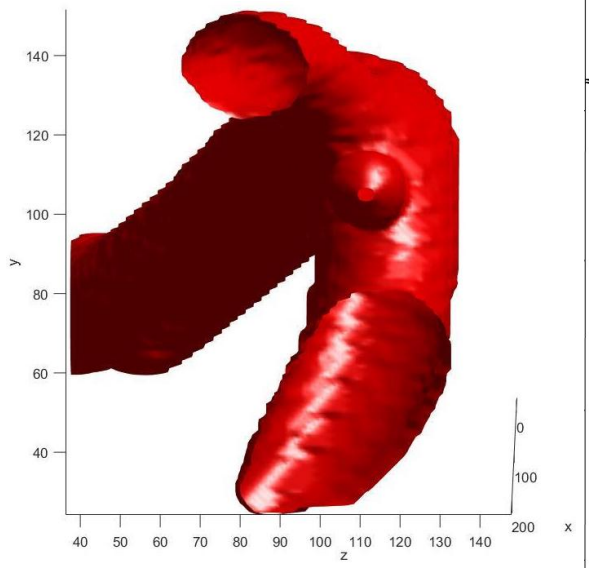

Figure 18: Visual representation of the z-axis

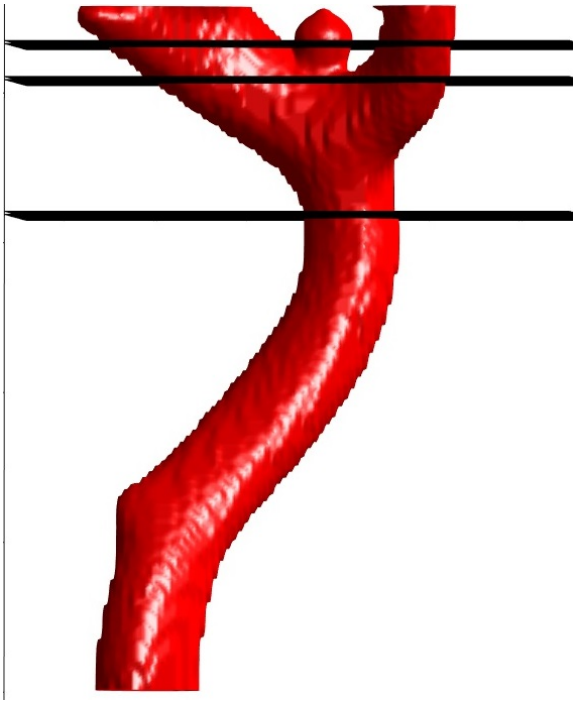

Figure 19: Visual representation of cross-sections

The average dimensionless shear stress $\tau^*_{mag,av}$, measured in specifically chosen cross-sections (x=160, x=205 and x=217) at the x-axis are presented in the figures below (see figures from section 5.1). The areas that were chosen represent cross-sections located right before the constructed aneurysm and on the constructed aneurysm, see figures 21 and 22 respectively. A cross-section through the region showing the highest average shear stress values in the figures above was also chosen, see figure 20.

The first graph shows a cross-section of average shear stress at the internal carotid artery before the bifurcation perpendicular to the flow direction, see figure 20. As we could see in the 3D-figures in section 5.1 the area in cross-section x=160 has a higher shear stress on the walls. This is apparent by the two peaks in figure 20. This section is not affected by the constructed aneurysm and shows similar values regardless if the aneurysm is present or not. Noticeable is the significant difference of average shear stress in the center of the vessel, whether the simulation was conducted with blood as a non-Newtonian fluid or not. The Newtonian simulations result in higher values of average shear stress, but both models show similar values of shear stress close to the vessel walls.

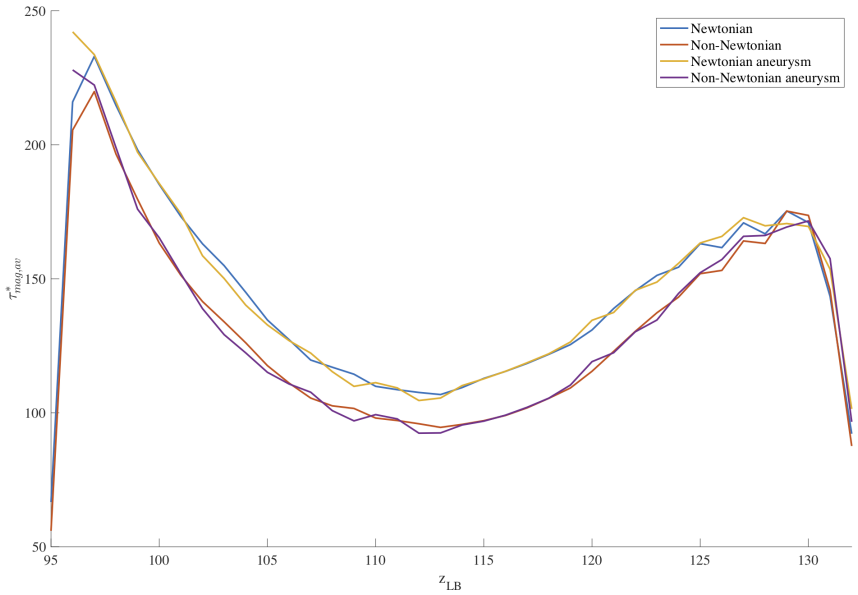

Figure 20: Cross-section 160, high shear stress area not in contact with constructed aneurysm

The graph of cross-section x=205 shows how the average shear stress is distributed right before the aneurysm begins. See figure 21. Since the vessel from this point onward is split into two, the profile of the function is not as symmetrical as in cross-section x=160 (see figure 20), due to fact that the walls separating the vessels have an impact on the average value of the shear stress.

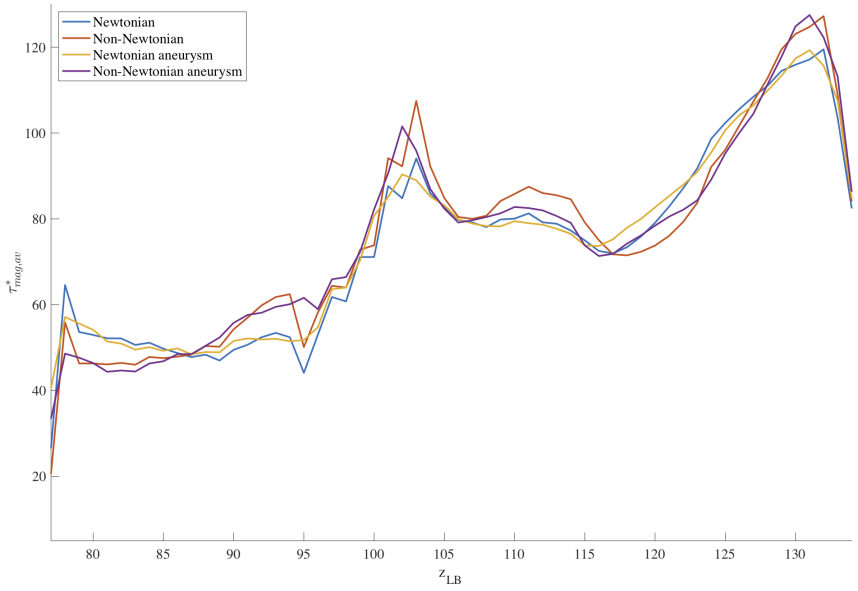

Figure 21: Cross-section 205, right before constructed aneurysm

The graph of cross-section x=217 shows how the average shear stress is distributed on the constructed aneurysm. See figure 22. In this cross-section we can notice a difference in average shear stress between with and without aneurysm in the area $104 < z < 118$ for both blood simulation models. However, the non-Newtonian model experiences significantly higher shear

rate in the area $110 < z < 118$, than the Newtonian model.

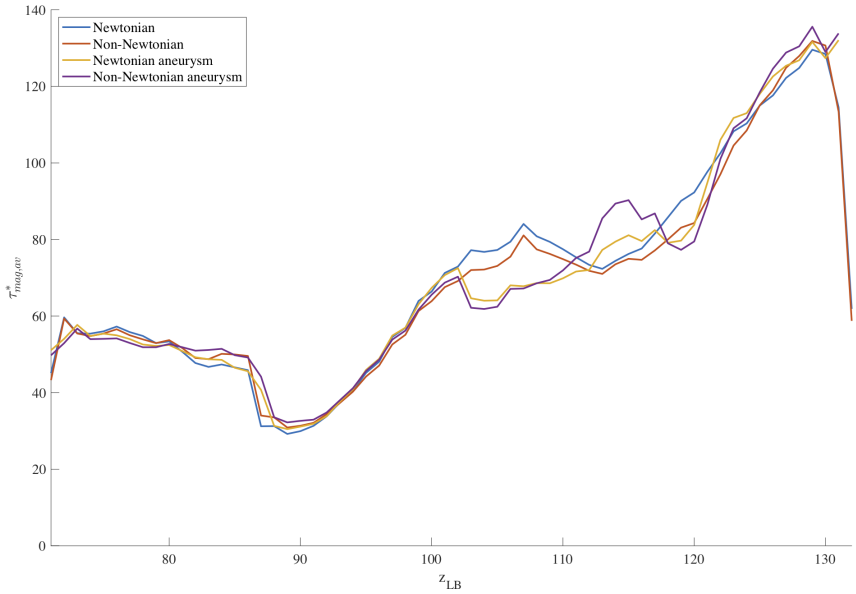

Figure 22: Cross-section x=217, on the constructed aneurysm

5.2 Total average shear stress

Figure 23 shows the average shear stress magnitude along the x-axis. The highest average is measured around cross-section x=160 indicating that the shear stress is high in the entire vessel in said cross-section. After the high shear stress region, the shear stress decreases until approximately x=210 where the bifurcation and constructed aneurysm occur, however, the average shear stress is lower than in cross-section x=160 indicating that the shear stress is low throughout the outer vessel walls not in contact with the bifurcation area. This can be seen in figure 15 and figure 16. The constructed aneurysm did not pose a significant change in the average magnitude of shear stress of the vessel.

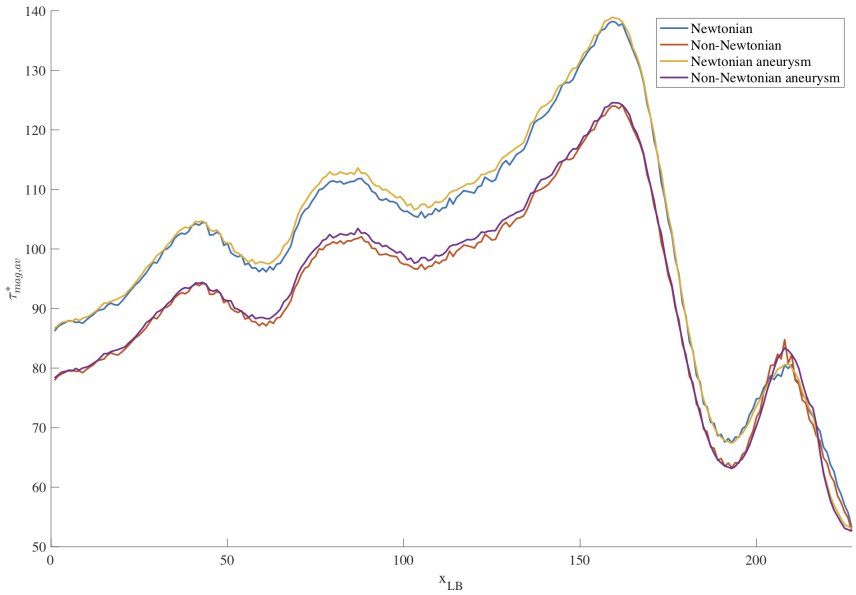

Figure 23: Average shear stress along x-axis

5.3 Velocity of the blood flow

Figure 24 and 25 present the dimensionless velocity of the blood flow only in the direction of the x-axis. The values are therefore affected by the size of the vessel, and the angle with respect to the x-axis, making it difficult to truly determine where the highest velocities are obtained without further investigation, however comparative investigations for the different simulations can be done.

Figure 24 and 25 represent the velocity of the blood flow for the Newtonian and the non-Newtonian case.

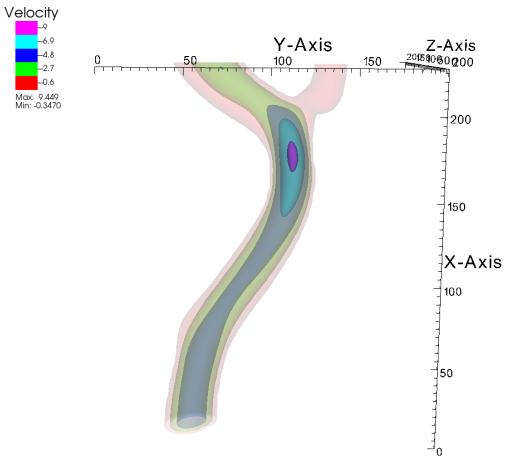

Figure 24: Velocity of the blood flow for Newtonian simulations

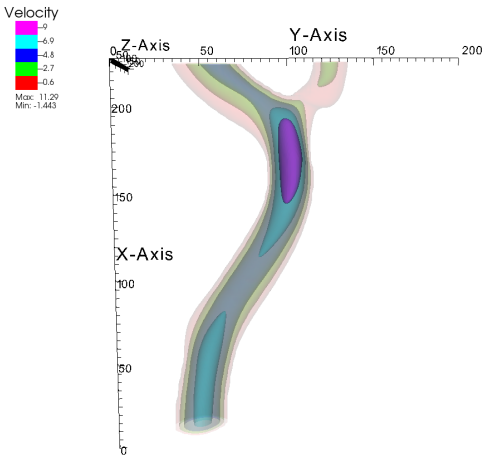

Figure 25: Velocity of the blood flow for non-Newtonian simulations

The most substantial difference between figure 24 and 25 is the increase of velocity specifically in the center of the vessel in the non-Newtonian simulation indicating evidence of shear thinning.

When investigating the velocity difference in the non-Newtonian simulations with and without the aneurysm, a velocity difference can be seen especially in the marked region. The constructed aneurysm is situated in the marked region implying it affects the velocity of the blood flow, see figure 26 and 27.

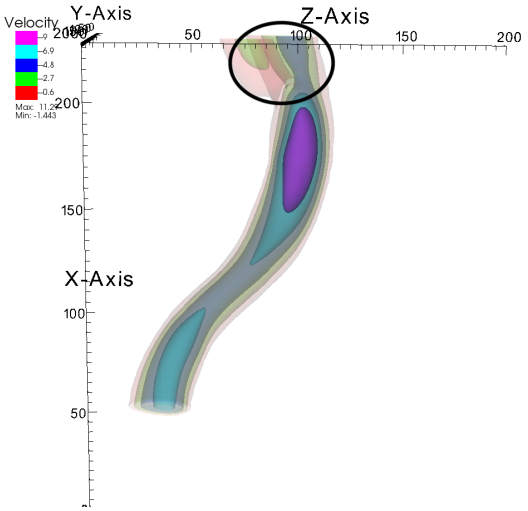

Figure 26: Velocity of the blood flow for non-Newtonian simulation without aneurysm in the XZ-plane

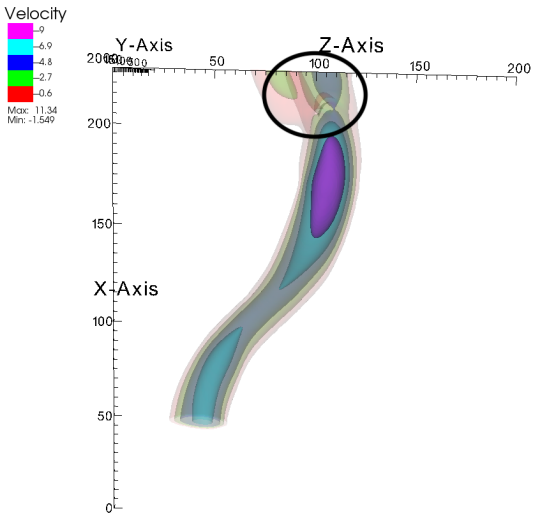

Figure 27: Velocity of the blood flow for non-Newtonian simulation with aneurysm in the XZ-plane

The average velocity in cross-section x=217, shows a difference in the region approximately around $104 < z < 118$, which is where the aneurysm is located (see figure 28). The average velocity decreases when the aneurysm is present thus confirming it disturbs the blood flow.

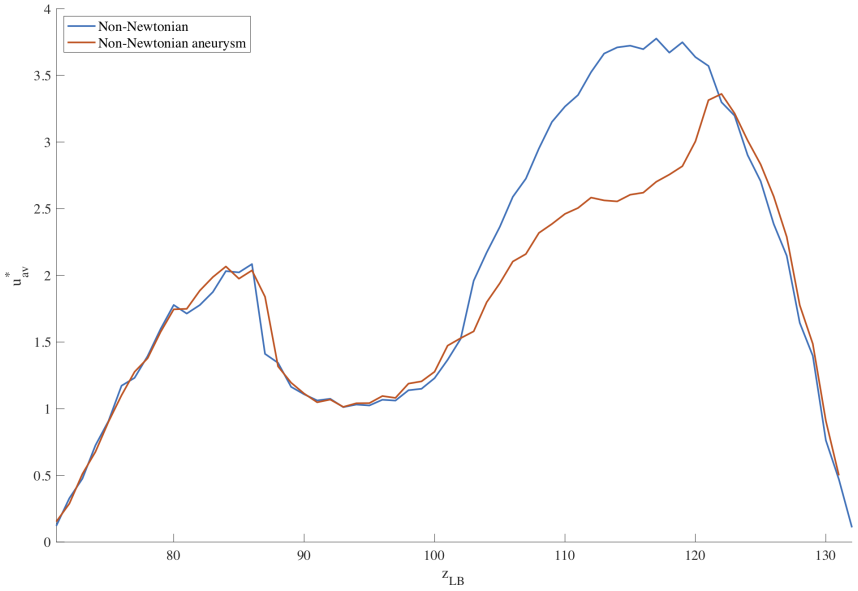

Figure 28: Average velocity at cross-section x=217 along z-axis with and without aneurysm for non-Newtonian simulations

Since figure 28 measures the average velocity, the velocity in the aneurysm must be significantly lower than in the rest of the vessel, this can be seen in figure 29 since there is only a small part of the aneurysm visible (in comparison to the full-sized aneurysm in figure 17), it indicates that a very low, or even stagnant flow is achieved in parts of the aneurysm, and are therefore not visible in the figure.

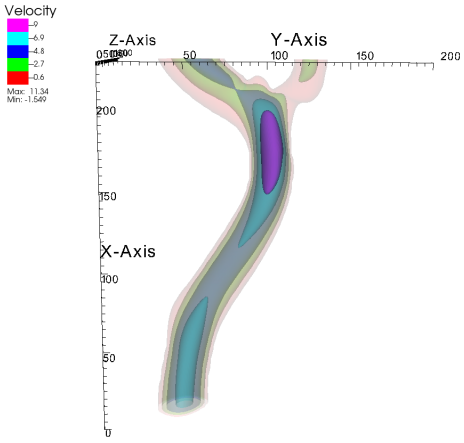

Figure 29: Velocity of the blood flow for non-Newtonian simulation with aneurysm in XY-plane

6 Discussion

6.1 Analysis of the hemodynamic parameters

As stated in section 3.2, the initiation of an aneurysm is most likely to occur in a bifurcation or where the blood vessel bends. This is due to the increased risk of endothelial dysfunction caused by the increased WSS, and flow velocity. In the simulations without the constructed aneurysm, it can be confirmed that the bifurcation, and the more bent part of the vessel at cross-section x=160 experience the highest values of WSS. This is clearly shown in the non-Newtonian 3D-figures 15 and 16. In a realistic setting the elastic nature of the artery would expand during such flow conditions thus decreasing the effect of high WSS. This is most likely one of those regions where WSS is overestimated due to rigid-wall model of the vessel walls. This result is also shown in figure 23, where you can see the highest peak around x=160. The reason why the peak associated with the bifurcation, after x=200, is relatively low compared to the peak at x=160, is because there is only a small area of high WSS in that region. The rest of the vessel in that area shows lower values of shear stress, lowering the average value.

By analyzing the cross-sections of average shear stress, it is possible to more precisely distinguish at which regions the high shear stress is located. Although, in areas with larger spans of shear stress it is harder to pinpoint. Looking at the area $104 < z < 118$, in cross-section x=217 in figure 22, it illustrates almost like a shift in the local peak between with and without aneurysm. Clearly the shear stress decreases in the first part of the area with the insertion of an aneurysm, and then increases at the end. This can also be shown in the 3D-figures in section 5.1 where it can be seen that the inserted aneurysm is very lightly coloured in pink (low shear stress) and at the left edge of it is dark blue spot (high shear stress). An explanation for the increase of shear stress at the edge of the aneurysm is that the bulge creates another small bifurcation. When analysing figures 16 and 14, one can see that the region with the highest WSS is situated on the edge of the constructed aneurysm, despite the average shear stress of this region resulting in lower values. Therefore the conclusions of a relation between high WSS and aneurysm initiation, still seems to be consistent with the results obtained in this thesis.

Following the results from section 5.2, a noticeable difference is observed between the Newtonian and non-Newtonian blood model, in the sense that the non-Newtonian blood exhibits shear-thinning behaviours that explain the higher velocities. This agrees well with the properties of a non-Newtonian fluid described in section 2, that the viscosity of blood is decreased under higher velocities compared to Newtonian blood that retains its constant viscosity.

When trying to distinguish areas at risk of aneurysm initiation, the use of a realistic blood flow model is crucial. When using a Newtonian model to analyze the blood flow we do not see the same peak in the bifurcation area as when looking at the non-Newtonian model. This is especially shown in cross-section x=205 (see figure 21) in the area right below the aneurysm, around the interval $104 < z < 118$. The non-Newtonian model without aneurysm shows a higher average shear stress value in the region compared to the Newtonian model without aneurysm. Also there is a much smaller change in shear stress between the two Newtonian functions compared to the two non-Newtonian functions. The overall average shear stress values are higher for the Newtonian models, this could lead to an overestimation of WSS. However, figure 22 shows that the Newtonian model underestimates the shear stress in the aneurysm, this could potentially lead to underestimating the risk of aneurysm rupture.

When comparing the two blood flow models with shear stress along the x-axis, see in figure 23, it shows how the non-Newtonian model takes on lower average shear stress values in most

regions except around x=220 where the the non-Newtonian model takes on a higher value. An explanation for this phenomenon is the shear thinning mechanism that the non-Newtonian model accounts for. As explained in section 2, at x=220 the RBCs elongate into ellipsoids and align with the flow. In such areas the non-Newtonian model displays a better flow than the Newtonian model, i.e. the value of the viscosity gets lower than in the Newtonian model.

6.2 Future directions

The results presented in the result section leaves many opportunities for further research. This section covers some of the future directions for developing more simulations.

6.2.1 Comparison of shear stress in geometries between two patients

The original plan was to include two patients in our thesis, BG0001 and BH0027. We were unable to investigate the hemodynamic for patient BH0027. Consequently it was not possible to compare the possible effect of anatomical variation between the two patients. For the sake of completeness, we here report a geometrical analysis and comparison of the CoW morphologies in figure 30. It shows the chosen segment of interest for such comparison between the two patients. It is clear that patient BH0027 has a less robust CoW, making this comparison worth exploring. However, in order to explore the proposed link between variations of CoW and aneurysm pathophysiology described in sections 3.4.1 and 3.4.2 the mere comparison of two geometry sections will not be enough. To give this geometrical difference a deeper meaning the simulation needs to contain more than just one segment of the CoW. We encourage the reader to look into the work done by Kristen Devault et. al that propose the modelling of the blood flow in the entire CoW [75]. Their approach is particularly insightful due to it allowing room for recalculation of flow patterns to compensate for the geometrical differences. We believe that incorporating their proposed models (that are validated against *in vivo* data) in future works will be a big step towards utilizing CFD for predictive studies such as ours.

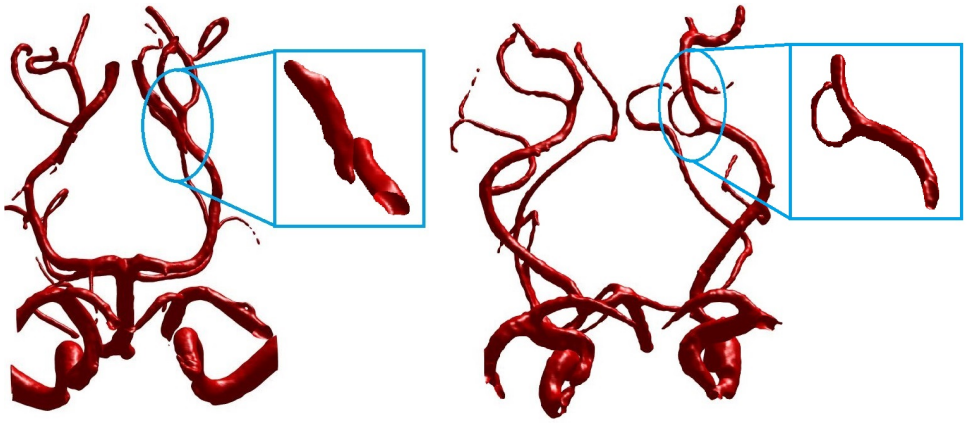

Figure 30: To the left CoW of BG0001, to the right CoW of BH0027. The blue circled area in BG0001 shows the geometry of the location corresponding to anterior cerebral artery in BH0027. Note that in BG0001 a bigger blood vessel connects to the right side of the CoW and has a symmetric equivalence on the left side of the CoW. The blue circled area in BH0027 shows the anterior cerebral artery. Note that the geometry of the anterior cerebral artery has no symmetric equivalence on the left side.

6.2.2 Improvements of the model

The present simulation framework is based on the assumption of rigid walls of the arterial vessels. This assumption has been shown to lead to almost 50 % overestimation of maximum WSS in some regions of CoW in previous studies [8].. Thus this feature seems to be essential for model accuracy. This overestimation could result in false diagnosis regarding risk zones for aneurysm formation. The disadvantage of applying the elastic model however, is indeed very time consuming, complex and perhaps outside the scope of a Bachelor thesis. One major drawback of rigid wall model is that it would be harder to draw a connection between biomechanics of the arterial wall reconstructions mentioned in 3.2 and 3.3 in the sense that a more dynamic model is able to capture the hemodynamic behaviour more accurately. The elastic nature of arterial walls also play an important role in absorbing some of the impacts of high blood pressure and velocities. We recommend reading the research paper on modelling arterial walls that takes into account the composition and features of an elastic vessel wall [27]. Perhaps a hybrid model of rigid and elastic wall will be suitable, where only the region of the artery containing the aneurysm is modelled as elastic.

There are many ways and computer programs to segment the cerebral circulation system. One of the methods is thresholding, used and applied in MATLAB in this report. As mentioned in section 4.1 this method provides an easy way to segment the blood vessels but also includes other unwanted parts of the brain. For getting even more accurate results of WSS analysis, it could be of interest to implement other methods and computer programs for segmentation.

Other interesting methods for image segmentation could be watershed, active contour, clustering, region growing and edge detection [73]. For example, the region growing approach is a iterative process that examines neighboring pixels to a chosen set of seed pixels. The neighboring pixels gets added if they have similar values to the seed pixels. The advantage of this method is that its easy to implement and a disadvantage of this method is that it will not work for non-smoothly varying regions. The image segmentation process could further be improved by applying morphological and filtering operations such as erosion and dilation.

As mentioned in sections 2.2 and 3.3 OSI and pulsating flow have been found significant. In order to study the effects of OSI, the flow needs to be pulsatile, i.e mimic the cardiac cycle. By accounting for the periodic change in flow conditions it would enable studying the turbulent nature of blood flow inside a constructed aneurysm. One argument that can be made in favour of not including pulsatile blood flow is based on the fact of the chronic nature of such vascular disease. It justifies the steady-flow assumption making the pulsating feature less significant over a long period of time. We however believe that by comparing a healthy cerebral vasculature with those containing aneurysms and/or defective CoW anatomy even in long-term research, would contribute to a more specific isolation of hemodynamic discriminators. It is suspected that several mechanisms may be involved in the growth and rupture process and simulating pulsating flow might offer interesting insights.

6.3 Ethical aspects

The ethical aspects of using CFD as a technique in the medical fields may be of interest since it provides *in silico* testing, meaning no direct use of animal testing will be necessary. The usage of animals for drug development and medical research increased in the 37 countries providing such statistics during the years of 2005-2015. With an estimated usage of animals reaching almost 200 million per year, this is an unsustainable and ethically questionable method that *in silico*

testing can reduce [76].

There is a lot of pros with *in silico* trials but it also comes with some ethical issues regarding the usage of data. The use and misuse of data is a widely discussed topic and events like the adoption of GDPR and the Facebook and Cambridge Analytical scandal has made the general population more aware of the topic and their rights regarding personal information. It has become more clear for people that the use of individual data needs to be under regulation [77]. Compared to *in vivo* or *in vitro* testing, *in silico* testing requires medical data collected from humans. This data can not be completely anonymized if wished to analyze whether the outcomes of the performed tests were as predicted. Gathering this type of personal information in a large extent give rise to several questions regarding appropriate use of health data [78].

Although the increased awareness, studies has shown that a majority of people are positive towards the use of personal data in medical research. A consultation regarding health data executed by the European Commission showed that on the statement "Citizens should be able to manage their own health data" over 93% of more than 1400 respondents agreed. On the statement "Sharing of health data could reveral beneficial to improve treatment, diagnosis and prevention of diseases across the EU" answered 83% of the participants that they agreed/strongly agreed. Another study made from asking clinical trial participants showed a difference in people's attitude towards sharing different types of data. It showed that people have a more positive attitude when it comes to sharing clinical trial data than clinical data (hospital data) [77].

7 Conclusions

The results from this project show that areas more prone to develop aneurysms experience higher WSS, supporting the connection between high WSS and aneurysm initiation. The results also indicate that the presence of an aneurysm affects the hemodynamics, the magnitude of the change depends on whether the simulations where made based on the Newtonian or non-Newtonian model. In the search of regions at risk for aneurysm initiation, both earlier researchers and our results suggest that the non-Newtonian model is more preferable in particular due to the ability of including shear thinning mechanism. Further research in areas such as anatomic variations in the CoW could give rise to new insights regarding crucial regions. Also, including OSI and pulsating flow, or applying a more elastic model in the simulation could be useful in future research.

References

[1] M. Patrice Lindsay et al. *World Stroke Organization (WSO): Global Stroke Fact Sheet 2019*. World Stroke Organization, 2020. URL: https://www.world-stroke.org/assets/downloads/WSO_Fact-sheet_15.01.2020.pdf.

[2] Per Wester and Margareta Norberg. "Cerebrovaskulära sjukdomar". In: (2018). URL: https://lakemedelsboken.se/kapitel/hjarta-karl/cerebrovaskulara_sjukdomar.html?fbclid=IwAR2ivv-uUmklJiONaUO8BkwonhRVqK7540-lgLGvy_gzOkV_x1erXQOvVo4.

[3] National Center for Chronic Disease Prevention, Division for Heart Disease Health Promotion, and Stroke Prevention. *Stroke Facts*. Sept. 2020. URL: https://www.cdc.gov/stroke/facts.htm.

[4] Isidro Ferrer and Noemi Vidal. "Neuropathology of cerebrovascular diseases". In: *Handbook of Clinical Neurology*. Vol. 145. 2018. DOI: 10.1016/B978-0-12-802395-2.00007-9.

[5] Physiopedia. *Subarachnoid Hemorrhage (SAH) — Physiopedia,* [Online; accessed 1-March-2021]. 2020. URL: https://www.physio-pedia.com/index.php?title=Subarachnoid_Hemorrhage_(SAH)&oldid=242569.

[6] Tianlun Qiu et al. "Association between hemodynamics, morphology, and rupture risk of intracranial aneurysms: a computational fluid modeling study". In: *Neurological Sciences* 38.6 (2017). ISSN: 15903478. DOI: 10.1007/s10072-017-2904-y.

[7] Marcelo A. Castro. "Understanding the Role of Hemodynamics in the Initiation, Progression, Rupture, and Treatment Outcome of Cerebral Aneurysm from Medical Image-Based Computational Studies". In: *ISRN Radiology* 2013 (2013). ISSN: 2314-4084. DOI: 10.5402/2013/602707.

[8] Haipeng Liu et al. "*State-of-the-Art Computational Models of Circle of Willis with Physiological Applications: A Review*". In: 8 (2020). ISSN: 21693536. DOI: 10.1109/ACCESS.2020.3007737.

[9] Joscilin Mathew, Parvathy Sankar, and Matthew Varacallo. "Physiology, Blood Plasma". In: *StatPearls* (2020). URL: https://www.ncbi.nlm.nih.gov/books/NBK531504/.

[10] Johann Schaller et al. "Blood Components". In: *Human Blood Plasma Proteins: Structure and Function*. John Wiley & Sons, 2008, pp. 7–16.

[11] Rohini Retarekar et al. "Stratification of a population of intracranial aneurysms using blood flow metrics". In: *Computer Methods in Biomechanics and Biomedical Engineering* 18.10 (2015), pp. 1072–1082. ISSN: 14768259. DOI: 10.1080/10255842.2013.869322.

[12] Jean Louis Vincent. "Understanding cardiac output". In: *Critical Care* 12.4 (2008), pp. 12–14. ISSN: 13648535. DOI: 10.1186/cc6975.

[13] Hippokration General Hospital and Athens Medical. "Vascular Wall Shear Stress: Basic Principles and Methods". In: *Hellenic J Cardiol* 46 (2005), pp. 9–15. URL: https://pubmed.ncbi.nlm.nih.gov/15807389/.

[14] F. Janoschek, F. Toschi, and J. Harting. "Simplified particulate model for coarse-grained hemodynamics simulations". In: *Physical Review E - Statistical, Nonlinear, and Soft Matter Physics* 82.5 (2010), pp. 1–12. ISSN: 15393755. DOI: 10.1103/PhysRevE.82.056710. arXiv: 1005.2594.

[15] Michael J. Simmonds, Herbert J. Meiselman, and Oguz K. Baskurt. "Blood rheology and aging." In: *Journal of geriatric cardiology : JGC* 10.3 (Sept. 2013), pp. 291–301. ISSN: 1671-5411. URL: http://www.ncbi.nlm.nih.gov/pubmed/24133519.

[16] Luca Lanotte et al. *A new look at blood shear-thinning*. 2016. arXiv: 1608.03730.

[17] T. Qui et al. "Association between hemodynamics, morphology, and rupture risk of intracranial aneurysms: a computational fluid modeling study". In: *Neurological Sciences* 38 (2017), pp. 1009–1018. DOI: https://doi.org/10.1007/s10072-017-2904-y.

[18] Poul M.F. Nielsen et al. *Computational biomechanics for medicine: Measurements, models, and predictions*. Springer International Publishing; 2018.

[19] William L. Hosch. *Encyclopaedia Britannica*. Aug. 2009.

[20] Paterson E. and Stern F. *Computational fluid dynamics*. AccessScience. McGraw-Hill Education; 2020.

[21] Shayan Naseri Nia et al. "Lattice Boltzmann simulation of natural convection heat transfer of a nanofluid in a L-shape enclosure with a baffle". In: *Results in Physics* 19 (Dec. 2020). ISSN: 22113797. DOI: 10.1016/j.rinp.2020.103413.

[22] "Simulation of stratified flows over a ridge using a lattice Boltzmann model". In: *Environmental Fluid Mechanics* 20 (5 Oct. 2020), pp. 1333–1355. ISSN: 1567-7419. DOI: 10.1007/s10652-018-9599-3. URL: http://link.springer.com/10.1007/s10652-018-9599-3.

[23] S Succi. *The Lattice Boltzmann Equation: For Fluid Dynamics and Beyond*. Oxford University Press; 2001.

[24] A. A. Mohamad. *Lattice Boltzmann method*. 2nd ed. Springer; 2019.

[25] James Welty, Gregory L Rorrer, and David G Foster. Fundamentals of Momentum, Heat and Mass Transfer. 6:e ed. John Wiley & Sons Inc; 2014.

[26] Elias Chalhoub et al. "Computational Fluid Dynamics of Human Cerebral Circulation Systems; A FluidMechanic Perspective". Unpublished.

[27] Frederico S. Teixeira et al. "Modeling intracranial aneurysm stability and growth: an integrative mechanobiological framework for clinical cases". In: *Biomechanics and Modeling in Mechanobiology* 19.6 (2020). ISSN: 16177940. DOI: 10.1007/s10237-020-01351-2.

[28] Theodora W.M. Raaymakers et al. "Mortality and morbidity of surgery for unruptured intracranial aneurysms: A meta-analysis". In: *Stroke* 29 (8 1998). ISSN: 00392499. DOI: 10.1161/01.STR.29.8.1531.

[29] F. Tomasello. "Asymptomatic aneurysms. Literature meta-analysis and indications for treatment". In: *Journal of Neurosurgical Sciences* 42 (1 SUPPL. 1 1998). ISSN: 00264881.

[30] Yuichi Murayama et al. "Computational fluid dynamics as a risk assessment tool for aneurysm rupture". In: *Neurosurgical Focus* 47.1 (2019). ISSN: 10920684. DOI: 10.3171/2019.4.FOCUS19189.

[31] Vitaliy L. Rayz and Aaron A. Cohen-Gadol. *Hemodynamics of Cerebral Aneurysms: Connecting Medical Imaging and Biomechanical Analysis*. 2020. DOI: 10.1146/annurev-bioeng-092419-061429.

[32] Nicolas K. Khattar et al. "Heparin treatment in aneurysmal subarachnoid hemorrhage: A review of human studies". In: *Acta Neurochirurgica, Supplementum*. Vol. 127. 2020. DOI: 10.1007/978-3-030-04615-6{_}3.

[33] "Management of unruptured intracranial aneurysms". In: *Neurology: Clinical Practice* 4.2 (Apr. 2014). ISSN: 2163-0402. DOI: 10.1212/CPJ.0000000000000019.

[34] Pengjun Jiang et al. "A Novel Scoring System for Rupture Risk Stratification of Intracranial Aneurysms: A Hemodynamic and Morphological Study". In: *Frontiers in Neuroscience* 12 (2018), p. 596. ISSN: 1662-453X. DOI: 10.3389/fnins.2018.00596. URL: https://www.frontiersin.org/article/10.3389/fnins.2018.00596.

[35] Li Liang et al. *Towards the Clinical utility of CFD for assessment of intracranial aneurysm rupture - A systematic review and novel parameter-ranking tool*. 2019. DOI: 10.1136/neurintsurg-2018-014246.

[36] David A. Steinman and Vitor M. Pereira. “How patient specific are patient-specific computational models of cerebral aneurysms? An overview of sources of error and variability”. In: *Neurosurgical Focus* 47.1 (2019). ISSN: 10920684. DOI: 10.3171/2019.4.FOCUS19123.

[37] Felicitas J. Detmer et al. “Development of a statistical model for discrimination of rupture status in posterior communicating artery aneurysms”. In: *Acta Neurochirurgica* 160.8 (2018). ISSN: 09420940. DOI: 10.1007/s00701-018-3595-8.

[38] Juhana Frösen. “Flow Dynamics of Aneurysm Growth and Rupture: Challenges for the Development of Computational Flow Dynamics as a Diagnostic Tool to Detect Rupture-Prone Aneurysms”. In: *Trends in Cerebrovascular Surgery*. Ed. by Tetsuya Tsukahara et al. Cham: Springer International Publishing, 2016, pp. 89–95. ISBN: 978-3-319-29887-0. DOI: 10.1007/978-3-319-29887-0_13. URL: https://doi.org/10.1007/978-3-319-29887-0_13.

[39] Marcello Longo et al. “Role of Hemodynamic Forces in Unruptured Intracranial Aneurysms: An Overview of a Complex Scenario”. In: *World Neurosurgery* 105 (2017), pp. 632–642. ISSN: 1878-8750. DOI: https://doi.org/10.1016/j.wneu.2017.06.035. URL: https://www.sciencedirect.com/science/article/pii/S1878875017309270.

[40] Mahsa Dabagh et al. “Hemodynamic and morphological characteristics of a growing cerebral aneurysm”. In: *Neurosurgical Focus FOC* 47.1 (1Jul. 2019), E13. DOI: 10.3171/2019.4.FOCUS19195. URL: https://thejns.org/focus/view/journals/neurosurg-focus/47/1/article-pE13.xml.

[41] “Medical gallery of Blausen Medical 2014”. In: *WikiJournal of Medicine* 1.2 (2014). ISSN: 20024436. DOI: 10.15347/wjm/2014.010.

[42] SEER Training Modules (U. S. National Institutes of Health National Cancer Institute). *Classification & Structure of Blood Vessels*. URL: https://training.seer.cancer.gov/.

[43] Anne M. Robertson and Paul N. Watton. “Chapter 8 - Mechanobiology of the Arterial Wall”. In: *Transport in Biological Media*. Ed. by Sid M. Becker and Andrey V. Kuznetsov. Boston: Elsevier, 2013, pp. 275–347. ISBN: 978-0-12-415824-5. DOI: https://doi.org/10.1016/B978-0-12-415824-5.00008-4. URL: https://www.sciencedirect.com/science/article/pii/B9780124158245000084.

[44] Nima Etminan et al. “Cerebral Aneurysms: Formation, Progression, and Developmental Chronology”. In: *Translational Stroke Research* 5.2 (Apr. 2014), pp. 167–173. ISSN: 1868-4483. DOI: 10.1007/s12975-013-0294-x.

[45] Dallas L. Sheinberg et al. “Endothelial dysfunction in cerebral aneurysms”. In: *Neurosurgical Focus* 47.1 (2019). ISSN: 10920684. DOI: 10.3171/2019.4.FOCUS19221.

[46] Nohra Chalouhi, Brian L. Hoh, and David Hasan. “Review of Cerebral Aneurysm Formation, Growth, and Rupture”. In: *Stroke* 44.12 (Dec. 2013). ISSN: 0039-2499. DOI: 10.1161/STROKEAHA.113.002390.

[47] Mannekomba R. Diagbouga et al. “Role of hemodynamics in initiation/growth of intracranial aneurysms”. In: *European Journal of Clinical Investigation* 48 (9 2018). ISSN: 13652362. DOI: 10.1111/eci.12992.

[48] A. J. Geers et al. “Wall shear stress at the initiation site of cerebral aneurysms”. In: *Biomechanics and Modeling in Mechanobiology* 16.1 (Feb. 2017), pp. 97–115. ISSN: 1617-7959. DOI: 10.1007/s10237-016-0804-3.

[49] H. Meng et al. “High WSS or Low WSS? Complex Interactions of Hemodynamics with Intracranial Aneurysm Initiation, Growth, and Rupture: Toward a Unifying Hypothesis”. In: *American Journal of Neuroradiology* 35.7 (2014), pp. 1254–1262. DOI: 10.3174/ajnr.A3558.

[50] Jennifer Chung et al. “Energy loss, a novel biomechanical parameter, correlates with aortic aneurysm size and histopathologic findings”. In: *Journal of Thoracic and Cardiovascular Surgery* 148 (3 2014). ISSN: 1097685X. DOI: 10.1016/j.jtcvs.2014.06.021.

[51] Takanobu Yagi et al. “Systematic review of hemodynamic discriminators for ruptured intracranial aneurysms”. In: *Journal of Biorheology* 33.2 (2019), pp. 53–64. DOI: 10.17106/jbr.33.53.

[52] Paolo Machi et al. “Hemodynamics of Focal Versus Global Growth of Small Cerebral Aneurysms”. In: *Clinical Neuroradiology* 29 (2 2019). ISSN: 18691447. DOI: 10.1007/s00062-017-0640-6.

[53] Daniel M. Sforza et al. “Hemodynamics in growing and stable cerebral aneurysms”. In: *Journal of NeuroInterventional Surgery* 8 (4 2016). ISSN: 17598486. DOI: 10.1136/neurintsurg-2014-011339.

[54] J. Pablo Villablanca et al. “Natural history of asymptomatic unruptured cerebral aneurysms evaluated at CT angiography: Growth and rupture incidence and correlation with epidemiologic risk factors”. In: *Radiology* 269 (1 2013). ISSN: 00338419. DOI: 10.1148/radiol.13121188.

[55] Takashi Inoue et al. “Annual rupture risk of growing unruptured cerebral aneurysms detected by magnetic resonance angiography: Clinical article”. In: *Journal of Neurosurgery* 117 (1 2012). ISSN: 00223085. DOI: 10.3171/2012.4.JNS112225.

[56] Philipp Berg and Oliver Beuing. “Multiple intracranial aneurysms: a direct hemodynamic comparison between ruptured and unruptured vessel malformations”. In: *International Journal of Computer Assisted Radiology and Surgery* 13.1 (2018). ISSN: 18616429. DOI: 10.1007/s11548-017-1643-0.

[57] Tao Wu and Qing Zhu. “Advancement in the haemodynamic study of intracranial aneurysms by computational fluid dynamics”. In: *Brain Hemorrhages* (2020). ISSN: 2589238X. DOI: 10.1016/j.hest.2020.12.002.

[58] Geng Zhou et al. “Association of wall shear stress with intracranial aneurysm rupture: Systematic review and meta-analysis”. In: *Scientific Reports* 7.1 (2017). ISSN: 20452322. DOI: 10.1038/s41598-017-05886-w.

[59] Ramanathan Kadirvel et al. “The influence of hemodynamic forces on biomarkers in the walls of elastase-induced aneurysms in rabbits”. In: *Neuroradiology* 49.12 (2007). ISSN: 00283940. DOI: 10.1007/s00234-007-0295-0.

[60] Bradley A. Gross et al. “Aspirin and aneurysmal subarachnoid hemorrhage”. In: *World Neurosurgery* 82.6 (2014). ISSN: 18788769. DOI: 10.1016/j.wneu.2013.03.072.

[61] James P B O’Connor. “Thomas Willis and the Background to Cerebri Anatome”. In: *Journal of the Royal Society of Medicine* 96.3 (2003). ISSN: 0141-0768. DOI: 10.1177/014107680309600311.

[62] Zvonimir Vrselja et al. “Function of Circle of Willis”. In: *Journal of Cerebral Blood Flow & Metabolism* 34.4 (2014), pp. 578–584. DOI: 10.1038/jcbfm.2014.7.

[63] J Rosner, V Reddy, and F Lui. “Neuroanatomy, Circle of Willis”. In: *StatPearls* (July 2020). URL: https://www.ncbi.nlm.nih.gov/books/NBK534861/.

[64] Zheng Hu Xu et al. “Morphological and clinical risk factors for the rupture of posterior communicating artery aneurysms: significance of fetal-type posterior cerebral artery”. In: *Neurological Sciences* 40.11 (2019). ISSN: 15903478. DOI: 10.1007/s10072-019-03991-4.

[65] Nebojša N. Stojanović et al. “Association between circle of willis configuration and rupture of cerebral aneurysms”. In: *Medicina (Lithuania)* 55.7 (2019). ISSN: 1010660X. DOI: 10.3390/medicina55070338.

[66] S. Iqbal. "A comprehensive study of the anatomical variations of the circle of Willis in adult human brains". In: *Journal of Clinical and Diagnostic Research* 7.11 (2013). ISSN: 2249782X. DOI: 10.7860/JCDR/2013/6580.3563.

[67] Bruno Coulier. "Morphologic variants of the Cerebral Arterial Circle on computed tomographic angiography (CTA): a large retrospective study". In: *Surgical and Radiologic Anatomy* (2021). ISSN: 12798517. DOI: 10.1007/s00276-020-02661-x.

[68] Qiong Fang et al. "Anatomic Variations of Circle of Willis and Its Compensatory Function Investigated by Computed Tomography Angiography". In: *Journal of Medical Imaging and Health Informatics* 8.4 (2018). ISSN: 2156-7018. DOI: 10.1166/jmihi.2018.2075.

[69] Bahman Jalali Kondori, Fateme Azemati, and Sonia Dadseresht. "Magnetic resonance angiographic study of anatomic variations of the circle of willis in a population in Tehran". In: *Archives of Iranian Medicine* 20.4 (2017). ISSN: 17353947.

[70] Nebojša Stojanović et al. "Presence of anatomical variations of the circle of Willis in patients undergoing surgical treatment for ruptured intracranial aneurysms". In: *Vojnosanitetski Pregled* 66.9 (2009). ISSN: 00428450. DOI: 10.2298/VSP0909711S.

[71] Jinyu Xu et al. "Morphological and Hemodynamic Analysis of Mirror Posterior Communicating Artery Aneurysms". In: *PLoS ONE* 8.1 (2013). ISSN: 19326203. DOI: 10.1371/journal.pone.0055413.

[72] Marcelo Valença et al. "Headache associated with intracranial aneurysms". In: *Headaches: Causes, Treatment and Prevention* (Jan. 2012), pp. 65–94.

[73] Anders Hedblom. "Blood vessel segmentation for neck and head computed tomography angiography". PhD thesis. Linköpings universitet, Tekniska högskolan, 2013. URL: http://urn.kb.se/resolve?urn=urn:nbn:se:liu:diva-101988.

[74] Asif Mehmood et al. "Finite Element Analysis on Bingham–Papanastasiou Viscoplastic Flow in a Channel with Circular/Square Obstacles: A Comparative Benchmarking". In: *Processes* 8.7 (2020). ISSN: 2227-9717. DOI: 10.3390/pr8070779. URL: https://www.mdpi.com/2227-9717/8/7/779.

[75] Kristen Devault et al. "Blood flow in the circle of willis: Modeling and calibration". In: *Multiscale Modeling and Simulation* 7 (2 2008). ISSN: 15403459. DOI: 10.1137/07070231X.

[76] Katy Taylor and Laura Rego Alvarez. "An Estimate of the Number of Animals Used for Scientific Purposes Worldwide in 2015". In: *Alternatives to laboratory animals : ATLA* 47.5-6 (2019). ISSN: 02611929. DOI: 10.1177/0261192919899853.

[77] Katharina Ó Cathaoir et al. *EU-STANDS4PM-Legal and ethical review of in silico modelling 2 Imprint Contact information*. Tech. rep. URL: https://www.eu-stands4pm.eu/lw_resource/datapool/systemfiles/elements/files/AA77832F664661DBE0537E695E8689E3/current/document/WP3_March2020_D3-1_V1_public.pdf.

[78] Francesco Pappalardo et al. "In silico clinical trials: concepts and early adoptions". In: *Briefings in Bioinformatics* 20.5 (Sept. 2019). ISSN: 1467-5463. DOI: 10.1093/bib/bby043.

DEPARTMENT OF MECHANICS AND MARITIME SCIENCES
DIVISION OF FLUID MECHANICS
CHALMERS UNIVERSITY OF TECHNOLOGY
Gothenburg, Sweden 2021
www.chalmers.se

CHALMERS
UNIVERSITY OF TECHNOLOGY